XI. PLASMA ELECTRONICS*

Prof. L. D. Smullin
Prof. H. A. Haus
Prof. A. Bers
Prof. W. D. Getty
Prof. P. Penfield, Jr.
Prof. D. J. Rose
Prof. T. H. Dupree
Prof. L. M. Lidsky
Prof. E. P. Gyftopoulos
R. R. Bartsch
W. L. Brassert
R. J. Briggs
T. S. Brown
J. F. Clarke
J. A. Davis
F. E. Dunn

P. Edmonds
M. R. Epstein
S. A. Evans
T. J. Fessenden
R. W. Flynn
E. T. Gerry
J. N. Hamawi
R. Hancox
B. A. Hartenbaum
C-F. G. Hsi
H. Y. Hsieh
G. I. Kachen, Jr.
C. A. Kapetanakos
B. R. Kusse
S. H. Kyong
M. A. Lieberman
M. Lind

J. D. Mills
D. L. Morse
A. A. Offenberger
K. C. Papadopoulos
R. R. Parker
L. M. Petrie, Jr.
S. Puri
J. A. Ross
H. M. Schneider
P. S. Spangler
C. C. Stewart
G. Theodoridis
E. Thompson
C. E. Wagner
R. N. Wallace
J. C. Woo

A. ELECTRON BEAM-PLASMA INTERACTION: SYSTEM C

In System C a high-perveance, hollow electron beam is injected axially into a magnetic-mirror system.[1] The beam generates a beam-plasma discharge[2] in the residual gas, which may be hydrogen, helium, or deuterium. The most important characteristics of the discharge are: (i) nearly complete ionization of the background gas in the immediate vicinity of the beam's path and appreciable "pumping" of the surrounding gas; (ii) the temperature of the electrons that comprise the majority of the plasma electrons is of the order of 100 ev; and (iii) an appreciable high-energy, non-Maxwellian tail of electrons with energies ranging from 10 kev to 200 kev.

The x-ray production of this plasma has been described in detail previously.[3] Further examination of x radiation has been made by making images of the x-ray source through a pinhole or slot. Other results presented in this report deal with diamagnetic field measurements, interferometric measurements of plasma density, and measurements of line broadening.

a. X-radiation Source

We found that considerably stronger x radiation was produced by the discharge in helium than in hydrogen. Relative strength is measured in terms of x-ray flux as detected with a sodium-iodide scintillator. Average flux rates are usually too low to detect with an x-ray survey meter. If x-ray production were from electron-ion collisions in the volume, then an increase by Z^2 would be expected. The radiation from the system

was detected by recording the fluorescence of a Type CB-2 fluorescent screen. This screen was adjacent to a Polaroid film sheet (ASA speed 3000) and both were held in a light-tight film holder. Exposures for periods as short as 5 minutes (corresponding to approximately 0.1 second of actual "on time") were made with the x radiation that penetrated the 0.120-inch wall of the stainless-steel tube. The relative positions of the film, fluorescent screen, and aperture are shown in Fig. XI-1. Without the lead shield in place we obtain an exposure that is limited by the copper magnet coil on each side as
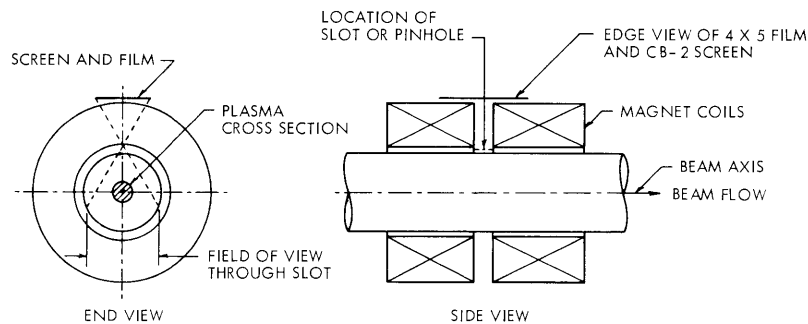

Fig. XI-1. Location of film and fluorescent screen. The slot in the lead shield is parallel to the beam's axis.

shown in Fig. XI-2a. With a slotted lead shield in place, we obtain an exposure as shown in Fig. XI-2b. The slot, which is 1/8 inch wide and 1 inch long, runs parallel to the axis of the plasma column. If a pinhole is used, the image is similar to that of Fig. XI-2b but restricted axially as expected. The stainless-steel tube filters out all but the hard radiation that is generated during the beam pulse. The scintillator indicated that most of the x-rays that produced the photographs of Fig. XI-2 were generated in three or four 10-20 μsec bursts during each beam pulse.

There are two possible interpretations of the x-ray image of Fig. XI-2b. The slot aperture indicates a narrow column for the radiation source, and implies that the radiation is from the plasma volume. Alternatively, we could interpret Fig. XI-2b as the result of radiation produced when the plasma column strikes the stainless-steel wall of the vacuum tube at points that are opposite the slot. This interpretation requires that the plasma strike the wall in the same place most of the time, which seems unlikely.

Photographs that are similar to Fig. XI-2a have been obtained recently for a beam-plasma discharge in deuterium gas, but no collimated photographs have been obtained.

It is necessary to carefully adjust the magnetic-field intensity, beam voltage, and gas pressure in order to obtain conditions under which the x radiation is strong enough to expose the film. In view of the potential importance of these photographs in locating the x-ray source, we plan to continue these measurements in greater detail.

EDGES OF MAGNET COILS

←— BEAM DIRECTION AND MAGNETIC AXIS

(a)

EDGES OF MAGNET COILS
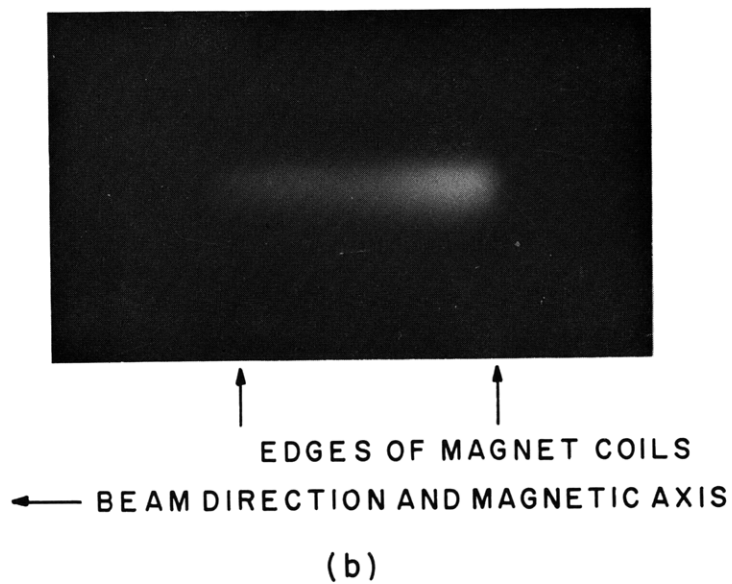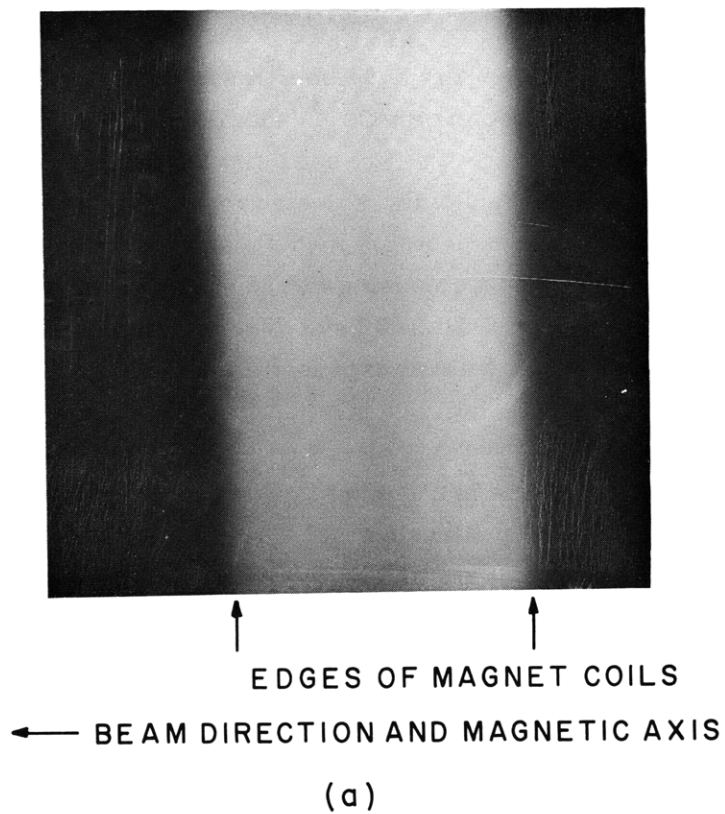
←— BEAM DIRECTION AND MAGNETIC AXIS

(b)

Fig. XI-2. Fluorescent-screen image of x-rays between two magnet coils. (a) With no collimating slot or pinhole. (b) With 0.125-inch collimating slot in a lead shield.

b. X-ray Energy

Further estimates of x-ray energy have been made by calibrating the scintillation detection system with the radiation from Cs^{137} (dominant γ-ray at 660 kev). A pinhole in a lead shield was used to reduce the flux until single photon pulses could be resolved. Two trials were made under randomly selected operating conditions. In each trial enough oscillograph traces were photographed to show from 500 to 700 scintillation pulses. All of these pulses occurred during the 350-μsec beam pulse. In each case the maximum energy was in the range 80-100 kev. The spectrum (number of counts versus energy) was roughly exponential with an exponentiation constant of 40 kev.

c. Spectral-Line Broadening

Several measurements of line broadening in helium and deuterium discharges were made by the method described by Hirschberg.[4] In this method the oscilloscope beam is intensified by a 5-μsec pulse that occurs at a preset sampling time during the beam pulse. The sampling time was set in our experiment to coincide with a strong burst of light or x-rays during the beam pulse. A Jarrell-Ash monochrometer was mechanically swept through the line at a rate of 1.25 Å per minute in synchronism with the horizontal oscilloscope sweep, which was 5 sec/cm. The resulting resolution of the line as shown on the oscilloscope was approximately 0.1 Å per centimeter. An example is shown in Fig. XI-3. Each vertical line corresponds to one 5-μsec sample of the light output of the monochrometer during a beam pulse. A total of 50-60 beam pulses was sampled
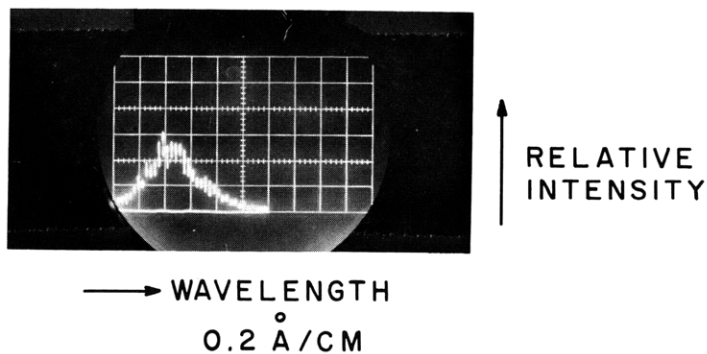

RELATIVE INTENSITY

WAVELENGTH
0.2 Å/CM

Fig. XI-3. He II 4686 Å line profile for typical conditions.

for Fig. XI-3. The height of the vertical line indicates the peak-to-peak variation of this output during the 5-μsec sample. Instrument broadening is approximately 0.3 Å. The 4686 Å He II line and several deuterium lines were investigated with this technique. The helium line is always broader than the instrument limit, but the indicated ion temperature is always less than 10 ev. Deuterium lines are also slightly broadened.

d. Interferometric Measurements of Density

A 3.5-mm microwave interferometer was set up for measurements of plasma density. The microwave beam is directed across the stainless-steel tube at a cross section near the midplane of the magnetic mirror. The two horns that are used for antennas are placed next to and transmit through 1-inch diameter glass ports in the stainless tube. A magic tee is used to recombine the signal from the two signal paths, and a phase shifter is placed in one arm for adjustments of the null. At the operating frequency of 93 Gc/sec the relation between density n and phase shift is

$$n = \left(\frac{\theta}{\pi}\right)(1.2 \times 10^{13}) \text{ electrons per cm}^3,$$

where θ is the phase shift in radians introduced by the plasma. A plasma diameter of 1 inch is assumed. The output of the interferometer's crystal detector is

$$v = V_{max} \sin^2 \frac{\theta}{2}.$$

Therefore the first maximum corresponds to $\theta = \pi$, the first null to $\theta = 2\pi$, and so on. An example of the interferometer output is shown in Fig. XI-4. The detector video
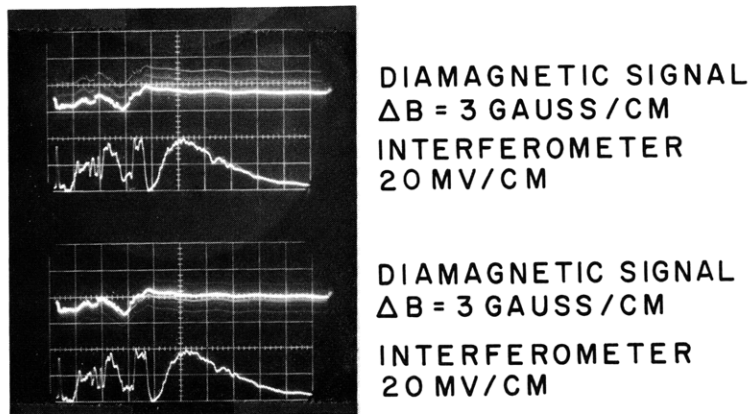

DIAMAGNETIC SIGNAL
ΔB = 3 GAUSS/CM
INTERFEROMETER
20 MV/CM

DIAMAGNETIC SIGNAL
ΔB = 3 GAUSS/CM
INTERFEROMETER
20 MV/CM

Fig. XI-4. Diamagnetic probe output and interferometer output for two beam pulses into deuterium plasma. Pressure, 1.5×10^{-3} torr; beam voltage and current, 17 kv and 13 amps; midplane field, 500 gauss; mirror ratio, 3.0; sweep rate, 200 μsec/cm; beam pulse length, 700 μsec.

bandwidth, which is probably 1-2 mc/sec, may smooth out some of the nulls and peaks. Typically, we find densities from 10^{12} cm^{-3} to a few times 10^{13} cm^{-3} indicated at gas pressures from 10^{-5} torr to 5×10^{-4} torr. The density is roughly proportional to pressure. Our estimate of a plasma diameter of 1 inch may be in error by a factor of two,

at most. Therefore a density of 10^{13} electrons/cm^3 may be considered typical. This is consistent with our previous estimates of density, which were based on measurements of the microwave radiation from the plasma.[5]

e. Diamagnetic Field Measurements

An operational amplifier with an open-loop gain of 2500 and bandwidth of 15 mc/sec was used for integration of the diamagnetic probe signals. The relationship between output voltage and magnetic field change is given by

$$v = \frac{NA\Delta B}{RC},$$

where RC = integrator time constant = 10^{-5} second

A = probe area = 0.7 cm^2

N = 50 turns

ΔB = flux change at the probe.

Using Hsieh's geometrical factor that relates the flux change at the probe to the flux change at the surface of the plasma, we have[6]

$$(\Delta B)_{probe} = \frac{b^2}{a^2} (\Delta B)_{plasma},$$

where a is the radial position of the probe, and b is the plasma radius. For our case $a^2/b^2 = 10$. The ratio of plasma energy density to magnetic-field energy density is given by

$$\beta = \frac{2}{B} \frac{a^2}{b^2} \frac{RCv}{NA},$$

where B is the steady-state magnetic field at the plasma surface. Using the integrator, we can measure v as a function of time. The frequency response is limited to 1 mc/sec by skin effect in the electrostatic shield around the probe. A large number of conditions has been investigated with the diamagnetic probe and the 3-mm interferometer at the same cross section (near the midplane of the magnetic mirror). The values of β observed thus far range as high as 0.6, and energy densities as high as 2×10^{15} ev/cm^3 have been measured. Since the density is near 10^{13} cm^{-3}, the indicated electron temperature is of the order of 100 ev. This order of temperature is found for most cases, although it may range as high as 1000 ev when the density is lower.

A strong correlation between pressure, density, and energy density has been observed. As the pressure is lowered toward 10^{-5} torr, the energy density increases and the density decreases, thereby indicating a higher electron temperature. Further quantative measurements of this effect are being made.

W. D. Getty

References

1. W. D. Getty and L. D. Smullin, System C: Strong interaction between a high-density, hollow electron beam and a plasma, Quarterly Progress Report No. 70, Research Laboratory of Electronics, M. I. T., July 15, 1963, pp. 114-116.

2. W. D. Getty and L. D. Smullin, Beam-plasma discharge: Buildup of oscillations, J. Appl. Phys. 34, 3421-3429 (1963).

3. W. D. Getty and L. D. Smullin, Observation of long confinement times of hot electron plasma in System C, Quarterly Progress Report No. 73, Research Laboratory of Electronics, M. I. T., April 15, 1964, pp. 58-62.

4. J. G. Hirschberg, Doppler temperatures in the C Stellerator, Phys. Fluids 7, 543-547 (1964).

5. L. D. Smullin, System C, Quarterly Progress Report No. 71, Research Laboratory of Electronics, M. I. T., October 15, 1963, pp. 115-116.

6. H. Y. Hsieh, Beam-plasma discharges: System A, Quarterly Progress Report No. 71, Research Laboratory of Electronics, M. I. T., October 15, 1963, pp. 111-115.

B. BEAM-PLASMA DISCHARGES: SYSTEM D

A new, larger, beam-plasma discharge experiment, System D, is being assembled. The new system is basically similar to the present System C,[1] but will utilize a discharge tube of larger diameter, stronger magnetic fields, and a lower base pressure. These changes are expected to increase the plasma containment time, and thus allow
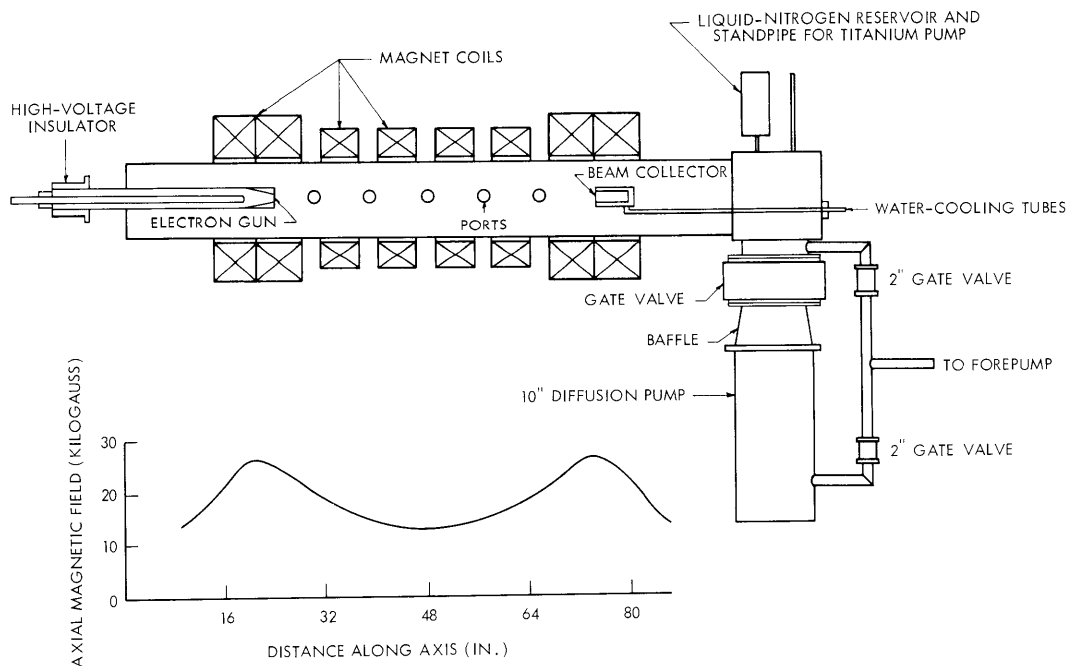

Fig. XI-5. Beam-plasma discharge, System D.

the production of denser plasmas. The better containment also may lead to more efficient heating of the plasma by the electron beam.

1. Magnet System

The magnetic field will be generated by 8 coaxial coils, as shown in Fig. XI-5. The four larger end coils are connected in series and carry a maximum current of 8800 amps. The four smaller center coils are also connected in series and carry a maximum of 1400 amps. The two series strings of magnets are connected in parallel across the generator, so that the ratio of the currents and hence the shape of the field, is unchanged as the field intensity is varied.

The maximum field that will be available on the axis of the system is shown at the bottom of Fig. XI-5. To obtain this field, 2.5 megawatts of electrical power and 460 gallons of water per minute will be required. Thus the experiment will be set up in the National Magnet Laboratory. The "mirror ratio" of 2:1 in the air-core system may be increased to ~3:1 in a region ~3 inches in diameter, with iron pole pieces. Delivery of the magnet system is scheduled for July 1, 1964.

2. Vacuum System

The discharge chamber is an aluminum tube, 12 inches in diameter and 8 feet long, with 1/4-inch wall thickness. As shown in Figs. XI-5 and XI-6, five ports, each 1 1/2 inches in diameter, are located on each side of the tube. The system is evacuated by a 10-inch oil-diffusion pump with a baffle cooled by liquid nitrogen. The pumping speed of this combination is approximately 2000 liters/sec.

The major sources of residual gas in the system are organic materials, such as the O-rings and gaskets. To minimize the outgassing, Viton O-rings have been used throughout the system and the two gaskets required (one at each end of the aluminum tube) have been cut from Butyl rubber sheet. With all parts of the system at room temperature, an ultimate vacuum of less than 2×10^{-7} torr is reached in three or four days. This pressure may be reached within 24 hours if the tube is heated with electrical heating tape to 100°C for several hours.

When liquid nitrogen is used in the baffle, the ultimate vacuum measured on the box above the pump drops to less than 2×10^{-8} torr. Two weeks of constant pumping were required to obtain this pressure. The pressure at the farthest part from the pump was less than 6×10^{-6} torr. To reduce the pressure difference between the ends of the tube, gaskets of Viton and Indium are being tried.

Experiments have been made with pumping by absorption of gas molecules on a thin film of titanium. The titanium is evaporated onto a cooled surface from a tungsten filament wound around a few titanium wires. The filament is located on the axis of a copper cylinder, 5 inches in diameter and 6 inches long. The assembly is suspended from
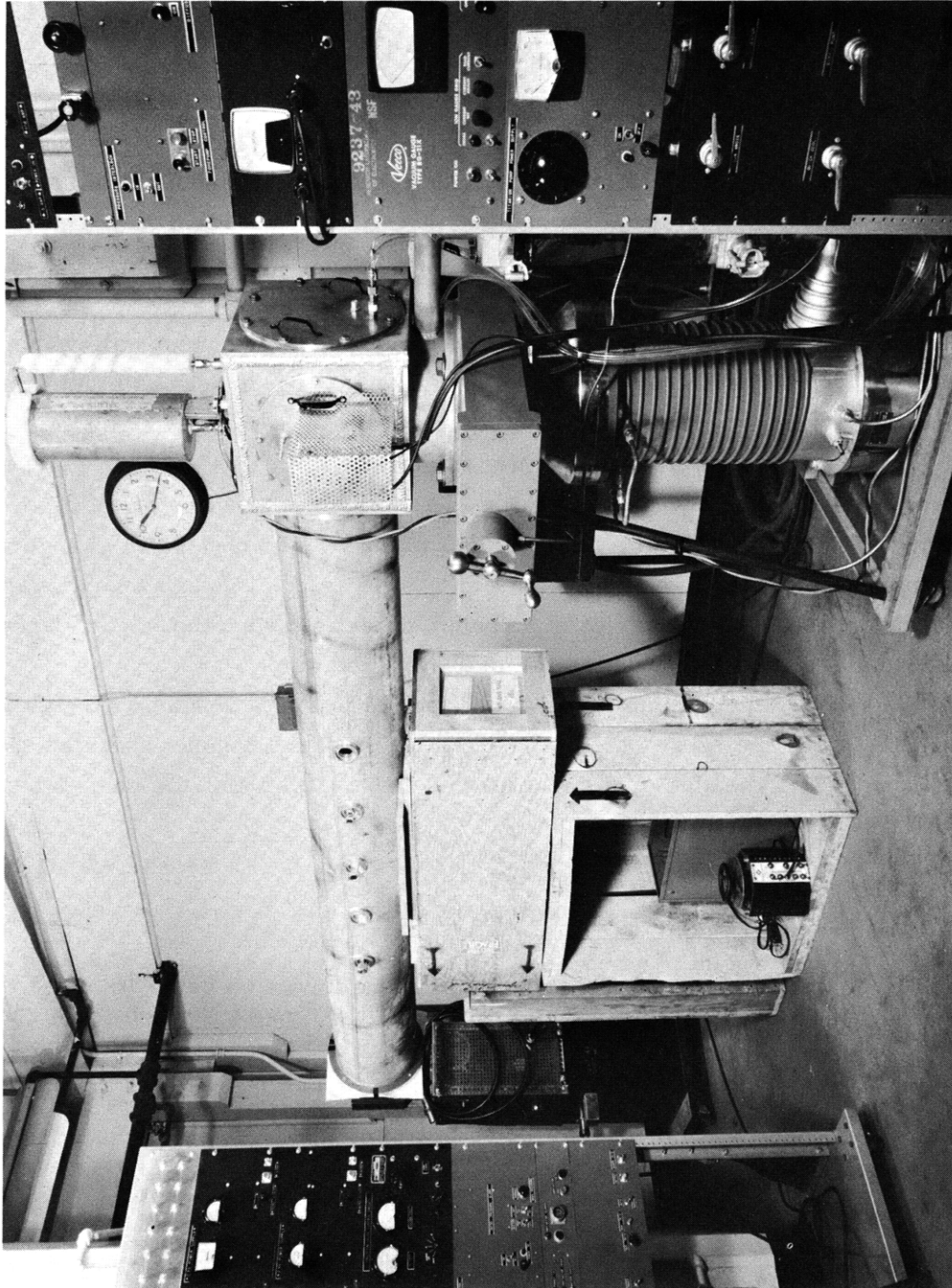
Fig. XI-6.   Vacuum system of System D.

the top of the box over the diffusion pump, and a reservoir for liquid nitrogen is located above the box. The pumping speed of this device has been found to be approximately 50 per cent of that of the baffled diffusion pump, in the pressure range obtainable in System D. This type of pump is most useful at pressures too low for efficient pumping by oil-diffusion pumps, and will probably not find great use in System D.

The 10 ports in the discharge chamber are to be used for investigating the plasma properties. They will carry devices such as coupling loops, electric probes, waveguide sections, magnetic probes, and clear quartz windows for light and x-ray studies. All of these devices are ready for use.

3. Electron-Beam System

The electron guns used in System D will be of the high-perveance, hollow-beam variety used in System C. The anode and mounting assembly are nearly complete, and will be ready when the cathode arrives. The collector is a water-cooled copper cylinder, closed at one end, and is now installed in the system.

The electronic circuitry for operating the electron gun is complete. A high-voltage DC power supply, with a maximum output of 150 ma at 27 kv, is used to charge a 700-μsec delay line. This delay line is discharged by a thyratron through the primary of a pulse transformer. The secondary of this transformer is connected to the electron-gun cathode, and supplies the voltage pulse for operating the gun.

Early in June 1964, the vacuum system will be taken to the National Magnet Laboratory and final tests will be made before the installation of the magnet system. The only major components still needed for operation of the system are the magnets and the electron-gun cathode assemblies.

D. L. Morse, L. D. Smullin

References

1. W. D. Getty, L. D. Smullin, System C: Strong interaction between a high-density, hollow electron beam and a plasma, Quarterly Progress Report No. 70, Research Laboratory of Electronics, M. I. T., July 15, 1963, pp. 114-116.

C. ION PLASMA OSCILLATIONS

We have measured amplification in the VHF range in a beam-plasma system. The ion plasma frequency ω_{pi} has been tentatively identified as the frequency of maximum amplification.

The experiment was described in Quarterly Progress Report No. 73 (pages 81-85). Briefly, it consists of injecting a modulated electron beam into a hot-electron plasma created by an electron-cyclotron resonance discharge (ECDR). The electron beam is

modulated at frequencies in the range 10-200 mc. The modulated beam current reaching the collector is then measured with a spectrum analyzer.

We observe a pronounced enhancement of the modulation when the hot-electron plasma is present. Figure XI-7 shows this enhancement as a function of frequency. The
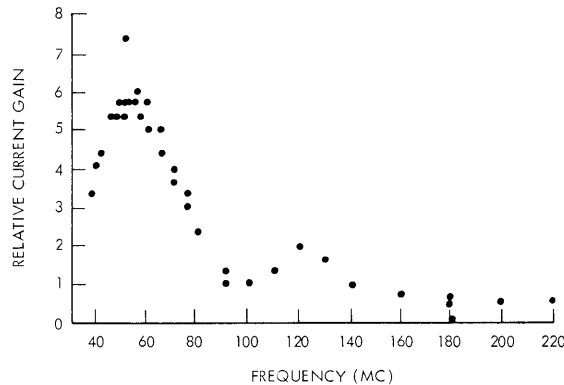

Fig. XI-7. Relative current gain vs frequency.

y coordinate is the ratio of the AC collector current when the hot-electron plasma is present to the AC collector current when the plasma is absent. The working fluid is hydrogen gas at a pressure of 5×10^{-5} torr. The base pressure is 10^{-6} torr. The power source for the ECDR is a cw 100-watt, 2.8-Gc magnetron. The electron beam operates at 250 volts, 4 ma; its diameter is estimated to be 1 mm. The interaction length (electron gun-collector separation) is approximately 20 cm.

It has not been possible to measure the electron density of the plasma directly. (Since it is generated by an RF discharge, one cannot use probes to measure n_0 without upsetting the discharge.) If one tentatively assumes, however, that in the steady state $\omega_{pe} = \omega_{ce}$, then for our conditions $\omega_{ce} = 2.8$ Gc, and for ω_{pi} it is ~65 mc. Figure XI-7 indeed shows a strong interaction near this frequency. Thus we tentatively identify the frequency of maximum interaction as the ion plasma frequency.

M. A. Lieberman, M. T. Vlaardingerbroek

D. INTERACTION OF AN ELECTRON BEAM WITH IONS IN A WARM PLASMA
OF FINITE TRANSVERSE DIMENSIONS

In a previous report we have shown that in a beam-plasma filled waveguide in which all electrons are confined by a strong axial magnetic field, and the plasma electron temperature (in volts) is large compared with the electron-beam DC voltage, a nonconvective instability near ion plasma frequency is obtained if the electron beam-plasma
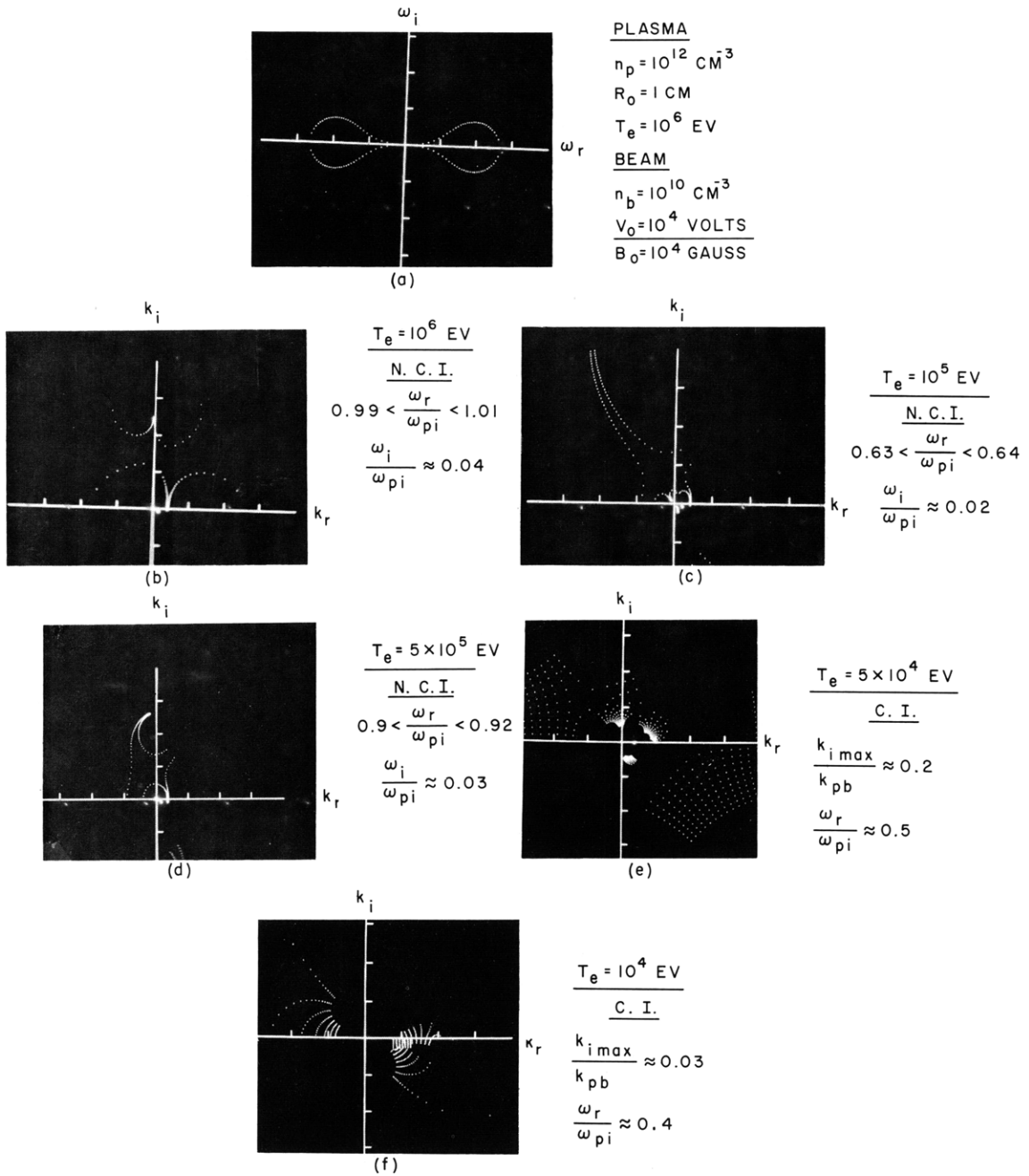
Fig. XI-8. (a) Contour of the real k axis in the complex ω plane. (b)-(f) Contours in the complex k plane of several constant real ω lines with ω_i varying from negative values to zero. In (b), (c), and (d) the real and imaginary parts of ω at the nonconvective instability (N. C. I.) are given. In (e) and (f) the maximum spacial growth rate of the convective instability (C. I.) and the frequency at which it occurs are given.

frequency exceeds the ion plasma frequency.[1] In this report we shall summarize the results of a thorough investigation of this instability as a function of plasma electron temperature and beam density. The newly developed instability criteria,[2] which we have now programmed for simultaneous computer analysis and display at M. I. T. Project MAC,[3] now make possible a rapid analysis of relatively complicated dispersion relations.

1. Dispersion Relation and Computer Results

The derivation of the dispersion relation has been given in a previous report.[4] For a time-space dependence $\exp j(\omega t - kz)$, where the waveguide axis is along the z-direction, we have

$$k^2 \left[1 - \frac{\omega_{pi}^2}{\omega^2} - \frac{\omega_{pe}^2}{\left(\omega^2 - k^2 v_{Te}^2\right)} - \frac{\omega_{pb}^2}{(\omega - kv_o)^2} \right] + p^2 \left[1 - \frac{\omega_{pi}^2}{\left(\omega^2 - \omega_{ci}^2\right)} \right] = 0. \tag{1}$$

A typical set of computer displays for the instability analysis in the complex-frequency plane and the complex wave-number plane is shown in Fig. XI-8. From such
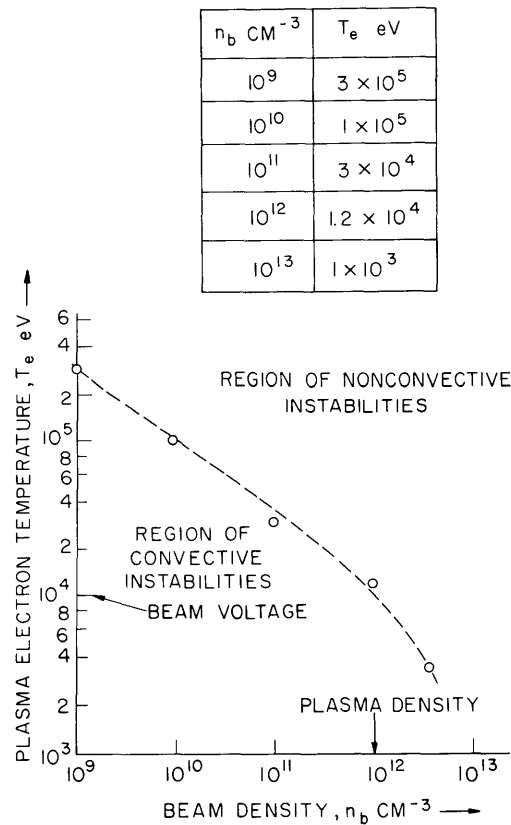
n_b CM^{-3}	T_e eV
10^9	3×10^5
10^{10}	1×10^5
10^{11}	3×10^4
10^{12}	1.2×10^4
10^{13}	1×10^3

Fig. XI-9. Relationship between beam density and electron temperature for the onset of the nonconvective instability.

displays we can determine the presence of a nonconvective instability (N. C. I.) and its growth rate in time (Fig. XI-8b-d), or the presence of a convective instability (C. I.) and its growth rate in space (Fig. XI-8e-f).

2. Characteristics of the Instability

A detailed stability analysis as described above and illustrated in Fig. XI-8 was carried out for a system with the following parameters:

Plasma density $\quad\quad n_p = 10^{12}$ cm^{-3}

Waveguide radius $\quad\quad a = 1$ cm

Electron-beam voltage $\quad V_0 = 10^4$ volts

Axial magnetic field $\quad B_0 = 10^4$ gauss.

The plasma electron temperature, T_e, and the electron beam density, n_b, were variable parameters. The results from several hundred observed displays of the complex-plane stability analysis are summarized in Figs. XI-9-11.

n_b	Ω_i	α	$\tau\,(\mu\text{SEC})$
10^9	0.002	2.6×10^6	0.4
10^{10}	0.016	21×10^6	0.05
10^{11}	0.025	33×10^6	0.03
10^{12}	0.032	42×10^6	0.025
10^{13}	0.03	40×10^6	0.025

$$\Omega = \frac{\omega_{imag}}{\omega_{pi}}$$

n_b	Ω_R
10^9	0.81
10^{10}	0.70
10^{11}	0.44
10^{12}	0.40
10^{13}	0.25
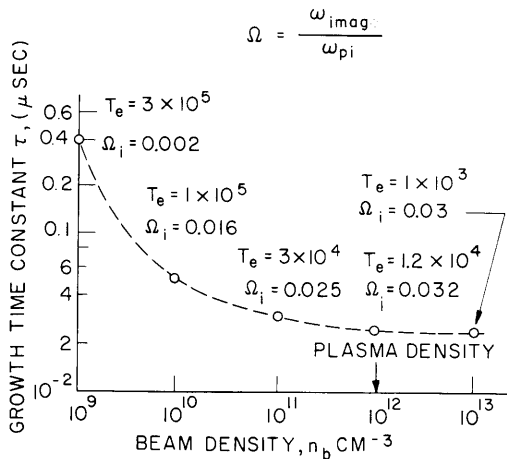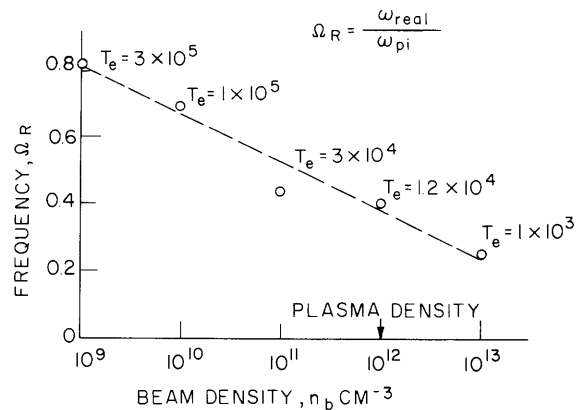
$$\Omega_R = \frac{\omega_{real}}{\omega_{pi}}$$

Fig. XI-10. Relationship between beam density and growth time constant at the onset of the nonconvective instability.

Fig. XI-11. Relationship between the beam density and the frequency at which the nonconvective instability occurs.

Figure XI-9 gives the required plasma electron temperature and beam density for the onset of the absolute instability. It shows that the required electron temperature may be reduced by increasing the beam density. The curve in Fig. XI-9 also gives the boundary between the occurrence of the nonconvective and the convective instabilities.

a. Nonconvective Instabilities

Figures XI-10 and XI-11, respectively, give the growth time constant and the real part of the frequency for the nonconvective instability. The e-folding times at the onset of the instability can be as short as 2×10^{-8} sec. The instability sets in at frequencies below the ion plasma frequency, and above the ion-cyclotron frequency.

n_b	Ω_i	α	τ (μ SEC)
10^{10}	0.035	47×10^6	0.022
5×10^9	0.02	27×10^6	0.036
10^9	0.005	6.6×10^6	0.15
6×10^8	0.005	6.6×10^6	0.15
3×10^8	0.0013	1.7×10^6	0.57

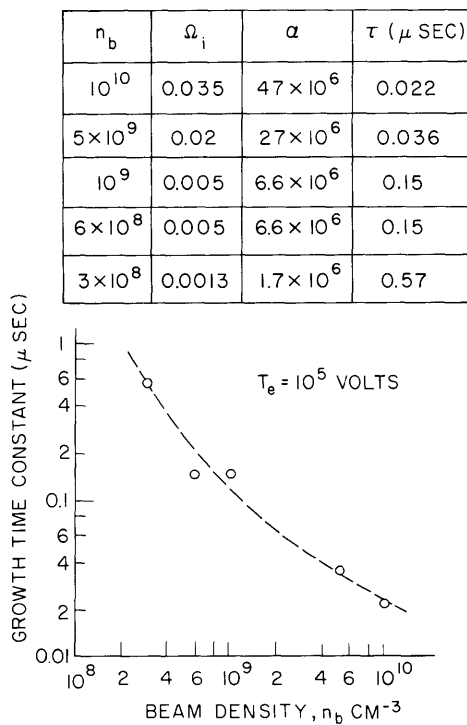| T_e	Ω_i	α	τ (μ SEC)
10^6	0.03	4.0×10^7	0.025
5×10^5	0.025	3.3×10^7	0.033
10^5	0.016	2.1×10^7	0.046

Fig. XI-12. Growth time constant of the nonconvective instability as a function of beam density at a fixed temperature.
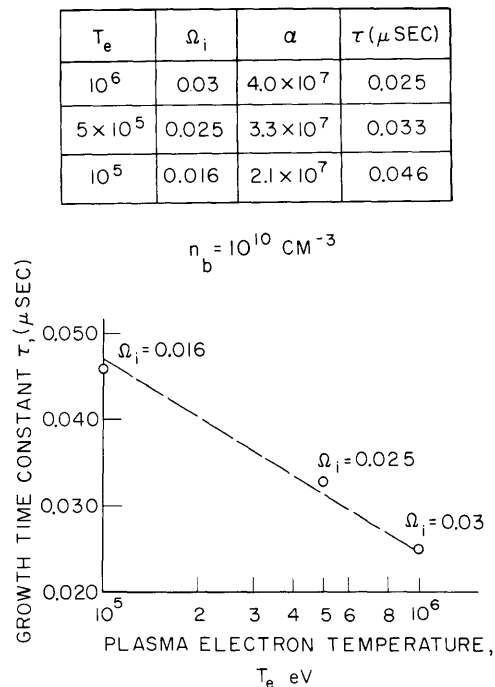
Fig. XI-13. Growth time constant vs plasma electron temperature at a fixed beam density.

Figures XI-12 and XI-13 illustrate the dependence of the time-growth rate upon beam density and plasma electron temperature.

b. Convective Instabilities

Figures XI-14 and XI-15 give the characteristics (gain-bandwidth) of the convective instabilities that are present below the threshold for the nonconvective instabilities
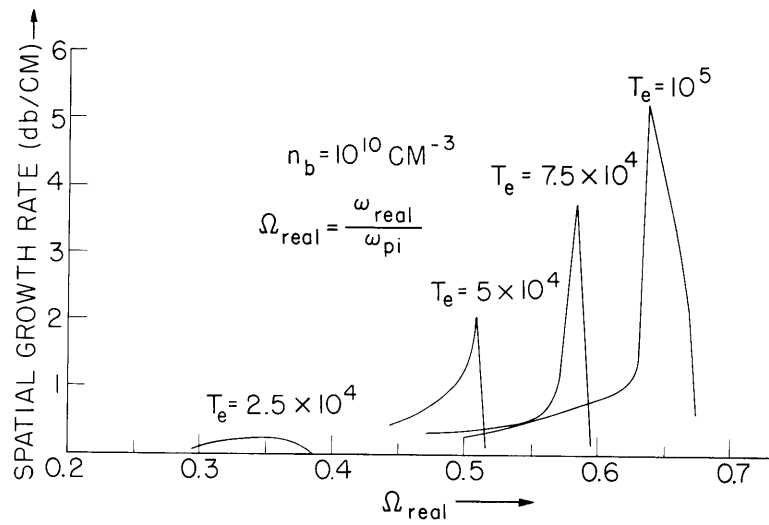
Fig. XI-14. Growth rate vs frequency as a function of temperature at a fixed beam density.

(see Fig. XI-9). The amplification rates are rather moderate and decrease rapidly with both plasma electron temperature and beam density.

c.   Frequencies of Strong Interactions

From Figs. XI-11, XI-12, XI-14, and XI-15 it is clear that the frequencies at which either the largest growth rate in time (for N. C. I.) or the largest growth rate in space (for C. I.) occurs are strongly dependent upon plasma parameters rather than on beam
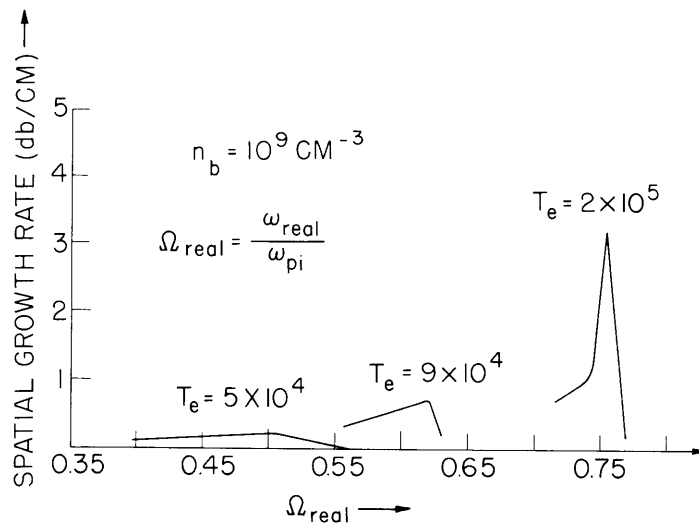

Fig. XI-15. Growth rate vs frequency as a function of temperature at a fixed beam density.

parameters. This is illustrated in Fig. XI-16. The solid line is the locus of frequencies at which the electron beam is in synchronism with the waves in the plasma waveguide, as illustrated in Fig. XI-17. We note that for low beam densities $(n_b \ll n_p)$
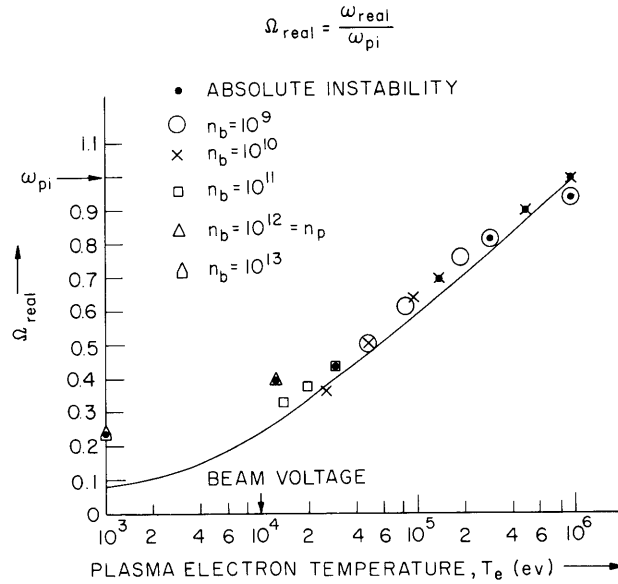

Fig. XI-16. Dependence of frequency of strong interaction (largest growth rate in space of a convective instability, or in time of nonconvective instability) on electron temperature for various beam densities.

this locus gives a good indication of the frequency of strongest interaction, as would be expected from weak-coupling arguments. We finally note that where the strong
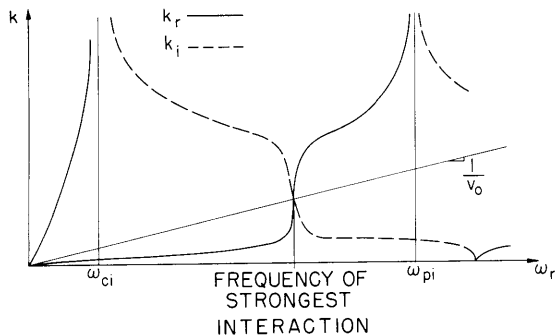

Fig. XI-17. Quasi-static dispersion characteristic of a plasma waveguide with hot electrons (Eq. 1 with $\omega_{pb} = 0$, pa = 2.4). (Figure not drawn to scale.)

interactions occur the waves in the plasma waveguide (Fig. XI-17) have a very low group velocity, and consequently we would expect a very high interaction impedance. Furthermore, the medium characteristics in that vicinity are inductive and hence

the plasma is strongly coupled to the beam. The low group velocity region of the hot-electron plasma waveguide can be traced to a coupling of the extraordinary wave with the ion plasma wave.

A. Bers, S. Puri, J. D. Mills

References

1. R. J. Briggs and A. Bers, Quarterly Progress Report No. 71, Research Laboratory of Electronics, M. I. T., October 15, 1963, pp. 131-137.

2. A. Bers and R. J. Briggs, Quarterly Progress Report No. 71, Research Laboratory of Electronics, M. I. T., October 15, 1963, pp. 122-131.

3. A. Bers and J. D. Mills, Quarterly Progress Report No. 73, Research Laboratory of Electronics, M. I. T., April 15, 1964, pp. 85-86.

4. R. J. Briggs and A. Bers, Quarterly Progress Report No. 70, Research Laboratory of Electronics, M. I. T., July 15, 1963, pp. 129-133.

E. DISPERSION DIAGRAMS FOR A WARM PLASMA

The results of hydrodynamic analyses[1,2] of the natural waves that propagate in an infinite collisionless electron-ion warm plasma immersed in a magnetic field will be displayed in terms of plots whose coordinates are wave number times the free-space
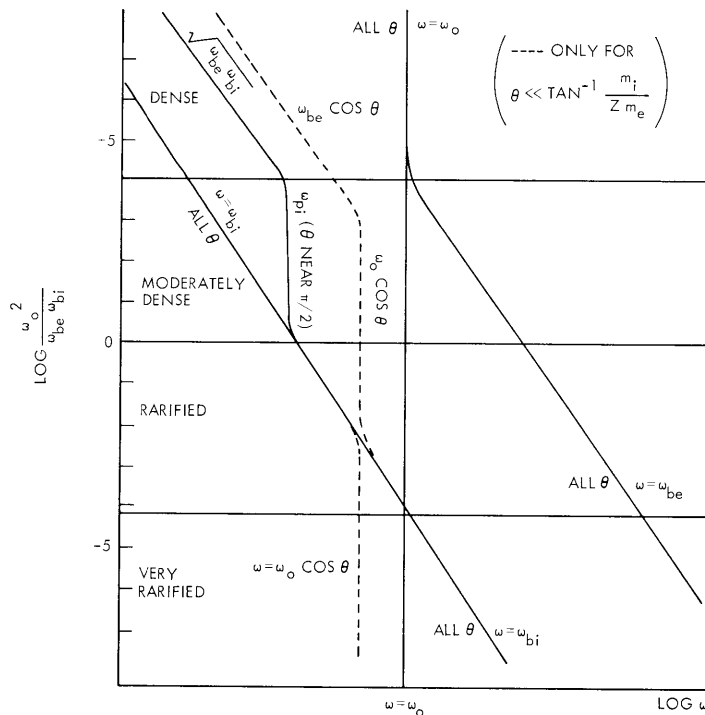

Fig. XI-18.   Approximate resonant frequencies in a cold plasma.

speed of light (kc) and frequency (ω), drawn for a fixed plasma density. This is done for arbitrary angle of propagation (θ) with respect to the applied magnetic field. Each plot is designed so that the kc-ω diagram for any chosen θ can be easily determined.

The shapes of the lines in the kc-ω plane are determined from the cold plasma
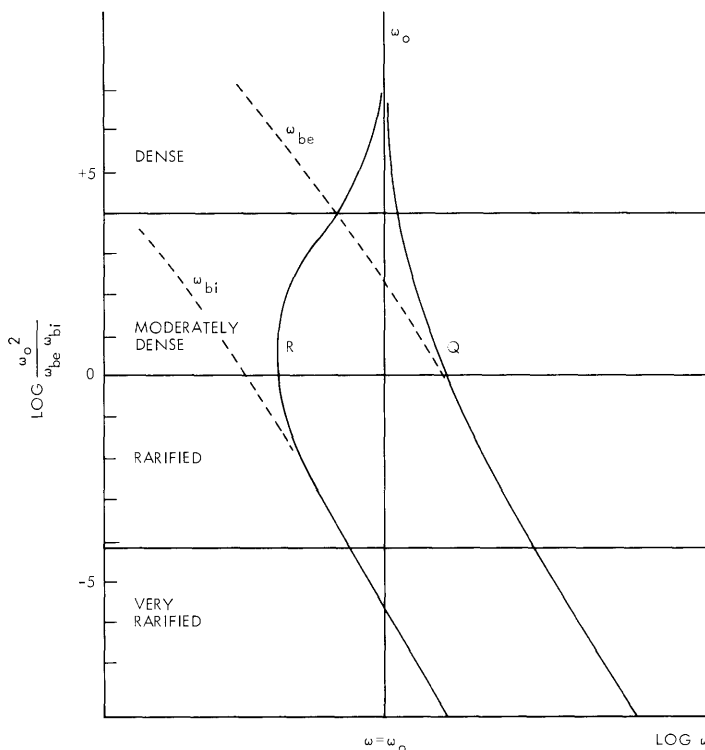

Fig. XI-19. Approximate cutoff frequencies in warm plasmas.

$$\left.\begin{array}{c}R\\Q\end{array}\right\} = 1/2\{[(\omega_{be}+\omega_{bi})^2+4\omega_o]^{1/2} \mp (\omega_{be}-\omega_{bi})\}.$$

resonances (k→∞), cutoffs (k→0), and asymptotes for low and high frequencies, as well as by coupling between waves. Figure XI-18 shows approximate resonant frequencies versus plasma density and magnetic field for a cold plasma.[2] In Fig. XI-19 we have shown the location of the cutoffs versus plasma density and magnetic field for a cold or warm plasma. In the hydrodynamic description the cutoffs are not temperature-dependent. We shall briefly discuss the form of the coupling. This also provides a means for visualizing wave changes as temperature effects are introduced into a cold-plasma description.

The dispersion relation for the hot plasma is eighth order in k. At all frequencies four waves exist either in propagating ($n^2 = k^2c^2/\omega^2 > 0$) or cutoff ($n^2 < 0$) mode. This

constitutes an addition of two waves more than the number that propagates in the cold plasma. These two additional waves can be identified as the longitudinal ($\bar{k} \parallel \bar{E}$) ion and electron waves, their names referring to the kind of particle whose motion dominates in the propagation of the wave. These waves are only distinct waves when $\bar{k} \parallel \bar{B}_0$. It has been shown by Allis, Buchsbaum and Bers[1] that, under the approximation $c \to \infty$, these waves can be defined from the dispersion relation for all θ. This approximation uncouples Maxwell's equations and limits propagation to the longitudinal waves.

The cutoff condition for these longitudinal waves is identical with the cold-plasma resonance condition. The resonance condition is identical with the cold-plasma right- and left-polarized wave resonance. Thus, we may view the hot plasma's kc-ω lines as slow, cold-plasma waves coupled to the longitudinal electron and ion plasma waves.

This approach is seen more clearly by comparing the lines in the kc-ω cold-plasma plots of Figs. XI-20 and XI-21 with the hot-plasma plots of Figs. XI-22 and XI-23. In these plots the following nomenclature is used for the waves in their uncoupled form. The terms for the hot-plasma waves are taken over from the cold-plasma names by relating similarly shaped kc-ω curves.
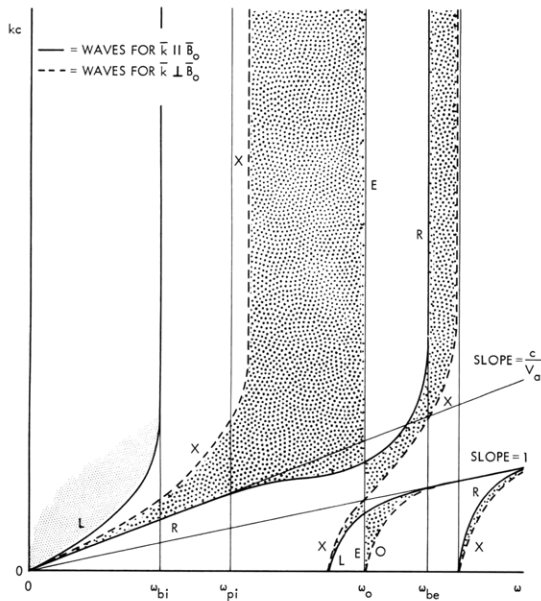

Fig. XI-20.

kc-ω diagram for oblique propagation in a cold plasma.

$$\frac{\omega_o^2}{\omega_{be}\omega_{bi}} = 100.$$
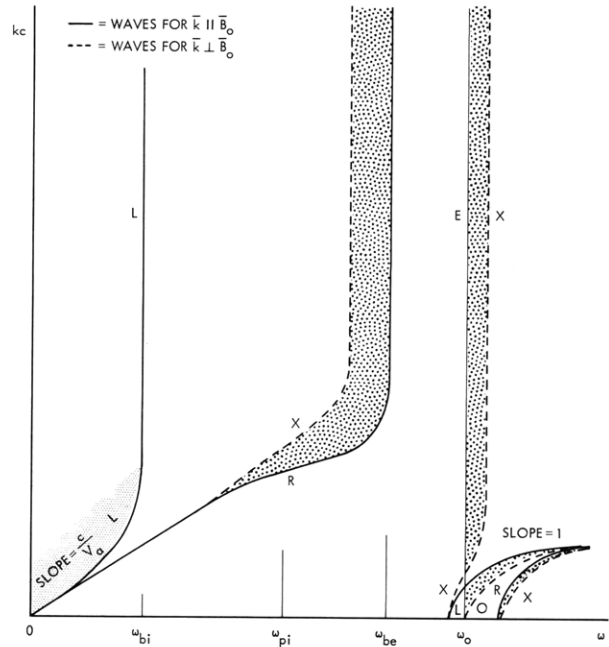

Fig. XI-21.

kc-ω diagram for oblique propagation in a cold plasma.

$$\frac{\omega_o^2}{\omega_{be}\omega_{bi}} = 10^6.$$

L = left-hand wave

R = right-hand wave

X = extraordinary wave

O = ordinary wave

E = electron plasma wave

I = ion plasma wave

V_e = electron thermal velocity = $(\gamma_e KT_e/m_e)^{1/2}$

V_i = ion thermal velocity = $(\gamma_i KT_i/m_i)^{1/2}$

V_a = Alfvén velocity = $c\left[1 + \left(\dfrac{\omega_o^2}{\omega_{be}\omega_{bi}}\right)\right]^{-1/2}$

V_s = plasma sound speed = $\left[\dfrac{\omega_{pi}^2 V_e^2 + \omega_{pe}^2 V_i^2}{\omega_o^2}\right]^{1/2}$.

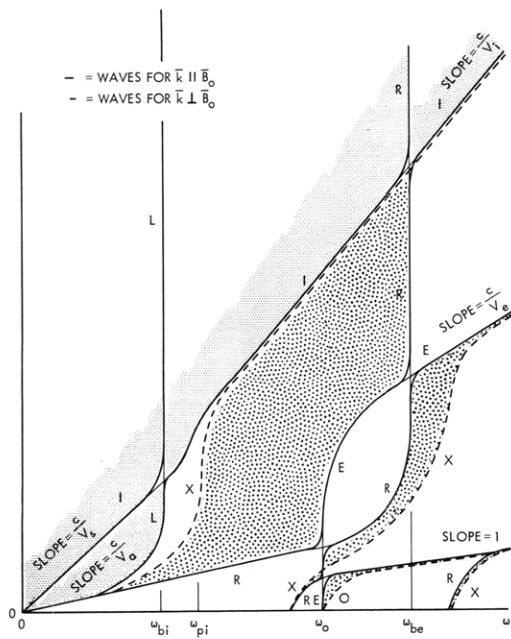Fig. XI-22.

kc-ω diagram for oblique prop-
agation in a hot plasma.
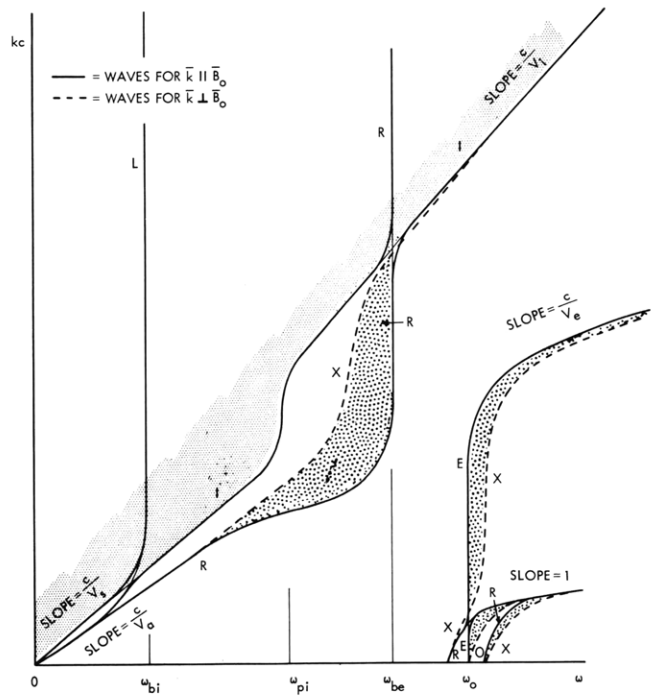
$\dfrac{\omega_o^2}{\omega_{be}\omega_{bi}} = 100.$

Fig. XI-23.

kc-ω diagram for oblique prop-
agation in a hot plasma.

$\dfrac{\omega_o^2}{\omega_{be}\omega_{bi}} = 10^6.$

The ratio of ion to electron mass has been taken as three so that linear scales may be used. Waves that propagate across ($\theta = 90°$) are shown as dashed lines. Waves that propagate along ($\theta = 0°$) are shown as solid lines. Cutoff waves are not shown. For $T_e = 0$, the electron plasma wave becomes the electron plasma resonance of the cold plasma. For $T_i = 0$, the ion plasma wave starts as in the general case but resonates at ω_{pi}.

Shaded regions between the kc lines for across and along propagation show how the lines shift as the propagation angle changes. The shading above the L and I lines indicates that these waves disappear for propagation across B_0. Their slopes at $\omega = 0$ vary as $(\cos \theta)^{-1}$. The location of the shaded regions for slow waves $\left(k > \dfrac{\omega}{c}\right)$ is determined by the approach discussed above.

In the fast-wave region, $\left(k < \dfrac{\omega}{c}\right)$, the dispersion diagram near ω_0 can be determined from a coupling of waves for θ near zero. The form of coupling is determined from the general hot plasma dispersion relation which for a very small value of θ takes the form:

$$D_T D_L = \delta(\overline{B}_0, \theta, \omega_{pe}, \omega),$$

where $D_T = 0$ represents solutions for waves with $\overline{k} \parallel \overline{B}_0 \perp \overline{E}$, and $D_L = 0$ represents those with $\overline{k} \parallel \overline{B}_0 \parallel \overline{E}$; δ is a coupling coefficient of order $\tan^2 \theta$. We assume θ is small enough so that the left-hand side of this equation does not change. The effect of the perturbation is only important in the neighborhood of points where waves of $D_T = 0$ cross those of $D_L = 0$. Near the point of coupling the dispersion relation takes the form

$$[k^2 - f(\omega)][k^2 - g(\omega)] = \frac{\delta}{[k^2 - h(\omega)][k^2 - e(\omega)]}, \tag{1}$$

where the left-hand side set to zero describes the two synchronous waves with no coupling. The denominator of the right-hand side set to zero is the dispersion relation for the two other waves that are far from the synchronous frequency of the first two waves. Hence, the right-hand side of the equation will be very small, because of the large values of $h(\omega)$ and $e(\omega)$, and near θ equal zero. It should be noted that for the hot-plasma dispersion diagrams there is always a fast-wave region ($k < \omega/c$) that is identical with the cold-plasma dispersion diagrams. The size of this region increases as temperature decreases.

This report is a summary of results that are presented in a thesis, entitled "Dispersion Relations for a Hot Plasma in a Magnetic Field," which was submitted by Marvin R. Epstein to the Department of Electrical Engineering, M. I. T., in partial fulfillment of the requirements for the degree of Master of Science.

M. R. Epstein, A. Bers

References

1. W. P. Allis, S. J. Buchsbaum, and A. Bers, Waves in Anisotropic Plasmas (The M. I. T. Press, Cambridge, Mass., 1963).

2. J. F. Denisse and J. L. Delcroix, Plasma Waves (Interscience Publishers, and John Wiley and Sons, Inc., New York, 1963).

F. A DEFINITION OF "PROPAGATION VELOCITY" OF UNSTABLE WAVES, AND RELATIONS BETWEEN THE SPATIAL AND TEMPORAL GROWTH RATES OF CONVECTIVE INSTABILITIES

1. Introduction

A formalism for distinguishing between amplifying and evanescent waves, and for determining absolute (nonconvective) instabilities was described in a previous report.[1] In the present report, some additional features about the propagation and growth of "unstable waves" are discussed. In this report, by the term "unstable wave" we mean a root of the dispersion relation of the system with a complex value of the frequency $\omega = \omega_r + j\omega_i$ (with $\omega_i < 0$) for a real wave number k, where the space-time dependence is $\exp j(\omega t - kz)$. Such "unstable waves" can correspond either to convective instabilities (amplifying waves) or nonconvective (absolute) instabilities.

The propagation of a pulselike disturbance on a uniform system is investigated in this report. It will be shown that a reference frame can always be found for which the disturbance increases exponentially with time at the maximum growth rate of any unstable wave, that is, at the maximum $(-\omega_i)$ for real k, and that this is the fastest possible growth rate in any frame. The velocity at which the observer must move to see this maximum growth rate in time is a sensible definition of the "propagation velocity" of the pulse on an unstable system. This velocity is given by $\partial\omega_r/\partial k$, with the derivative evaluated at the point of the maximum negative imaginary part of $\omega(k)$ for real k.

In the procedure outlined before for determining amplifying and evanescent waves, it is clear that a necessary condition for a system to support amplifying waves is that "unstable-wave" solutions be obtained from the dispersion equation.[1] For a system that is free from absolute instabilities, the question whether this condition insures that there is an amplifying wave solution for some real frequency, that is, that the condition is sufficient as well as necessary, still remains. Sufficiency is proved in this report. It is shown that for a system that supports only convective instabilities, the maximum amplification rate in space must be greater than the maximum growth rate in time (maximum $(-\omega_i)$ for real k) divided by the "propagation velocity" defined below. Also, if it is known a priori that the maximum amplification rate is less than infinity, then a definite upper bound for this amplification rate in terms of the temporal growth rate can also be given.

2. Propagation of a Pulse Disturbance

In the previous report,[1] the character of the response $\psi(z, t)$ was investigated in the asymptotic limit $t \to \infty$ for finite values of z. Physically, it is quite clear that the distinction between convective and nonconvective instabilities is always with respect to a given reference frame, since a moving observer might "keep up" with a convective instability and thus see a response increasing indefinitely with time. To investigate this, we shall study the response to an impulse source, $s(z, t) = \delta(z)\, \delta(t)$, in the limit as $t \to \infty$ and $z \to \infty$ with

$$z = Vt + z_0, \tag{1}$$

where V is a certain fixed velocity and z_0 remains finite. (We could, of course, handle this problem by a transformation into a moving reference frame. We choose not to do this, because of the complications introduced by a relativistically correct transformation. The asymptotic response that we calculate, therefore, is the one measured in the laboratory frame with the laboratory time t, when the "measuring instrument" moves at velocity V.)

The impulse response of the system[1] is given by

$$\psi(t, z) = \int_L \frac{d\omega}{2\pi} \int_F \frac{dk}{2\pi} G(\omega, k)\, e^{j(\omega t - kz)}, \tag{2}$$

where the "system function" $G(\omega, k)$ has poles at the zeros of the dispersion equation, and the integrations are over the appropriate Laplace and Fourier contours.

To investigate this response in the asymptotic limit $t = z/V \to \infty$, we write $\psi(t, z)$ as a function of t and z_0, with $z(t)$ given by Eq. 1. This can be written

$$\psi(t, z_0) = \int_L F'(\omega', z_0)\, e^{j\omega' t} \frac{d\omega'}{2\pi} \tag{3}$$

with

$$F'(\omega', z_0) = \int_F G'(\omega', k)\, e^{-jkz_0} \frac{dk}{2\pi} \tag{4}$$

$$\omega' = \omega - kV \tag{5}$$

and

$$G'(\omega', k) = G(\omega' + kV, k). \tag{6}$$

From Eqs. 3 and 4 the computation of the response $\psi(t, z_0)$ as $t \to \infty$ proceeds in exactly the same manner as for $\psi(t, z)$ with $t \to \infty$, except that ω is replaced by ω'.

If the plot of complex ω for <u>real</u> k obtained from the dispersion equation is as shown in Fig. XI-24, where σ_o is the maximum growth rate of <u>any</u> unstable wave, then the choice of $V = V_o = (\partial\omega_r/\partial k)_o$ leads to a saddle point of $\omega'(k)$ at k_o, since

$$\frac{\partial\omega'}{\partial k} = \frac{\partial\omega_r}{\partial k} - V_o + j\frac{\partial\omega_i}{\partial k}$$

$$= 0 \text{ at } k = k_o. \tag{7}$$

This is equivalent to a merging of two roots of k (obtained from the dispersion equation) into a double root on the real k axis as the frequency ω' approaches $\omega'_{r_o} - j\sigma_o$
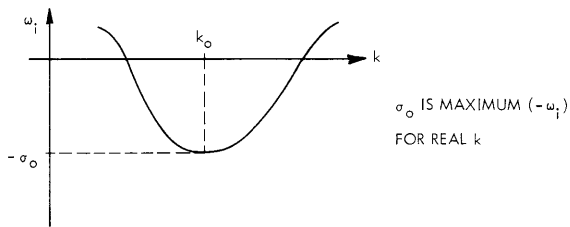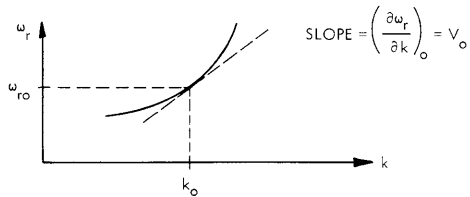

σ_o IS MAXIMUM $(-\omega_i)$
FOR REAL k

Fig.   XI-24.   Sketch of complex ω for real k.

SLOPE $= \left(\dfrac{\partial\omega_r}{\partial k}\right)_o = V_o$

(Fig. XI-25). This merging of the roots of k will lead to a singularity of $F'(\omega', z_o)$, and therefore to a response that increases as $\exp(\sigma_o t)$ if the roots are merging
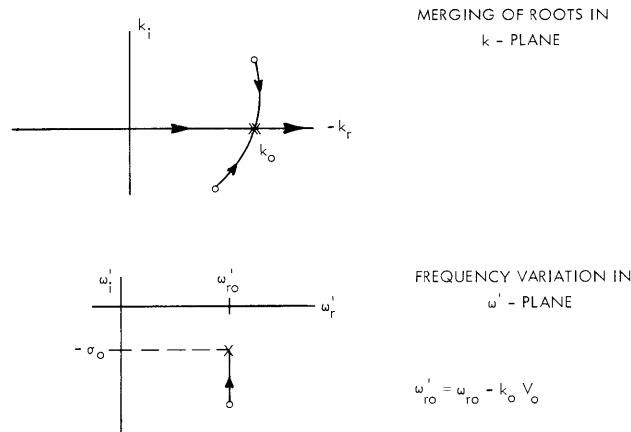

MERGING OF ROOTS IN
k - PLANE

FREQUENCY VARIATION IN
ω' - PLANE

$\omega'_{ro} = \omega_{ro} - k_o V_o$

Fig.   XI-25.   Merging of roots on real k axis.

through the $\widetilde{F}$ contour.[1]

To show that this is the case, we first note that the maximum negative imaginary part of $\omega'(k)$ for real k is also equal to σ_o, since $\operatorname{Im} \omega' = \operatorname{Im} \omega$ for real k (Eq. 5). For this reason, no roots of k from the dispersion relation can have crossed the real k axis for $\operatorname{Im} \omega' < -\sigma_o$, and therefore the $\widetilde{F}$ contour is the Fourier contour (the real k axis) for $\operatorname{Im} \omega' < -\sigma_o$. This merging of the roots therefore must be taking place through the Fourier contour as shown in Fig. XI-25, and this leads to a branch-pole singularity of $F(\omega', z_o)$ at frequency $\omega' = \omega'_{r_o} - j\sigma_o$, and consequently to a response that increases as $\exp(\sigma_o t)$. (One might worry about the special case in which the merging poles just "graze" the real k axis; however, the approach of ω to the saddle point can be at any angle — not just at 90° to the real-ω axis as shown in Fig. XI-25.)

It is also obvious from this analysis that no value of V can lead to an asymptotic response that increases faster than $\exp(\sigma_o t)$.

3. Relations between Spatial and Temporal Growth Rates of Convective Instabilities

We consider now a system that has no absolute instabilities, and is driven by a source of the form $s(z, t) = \delta(z) f(t)$. The response can then be written

$$\psi(t, z) = \int_{-\infty}^{\infty} F(\omega, z)\, f(\omega)\, e^{j\omega t} \frac{d\omega}{2\pi}, \tag{8}$$

where

$$F(\omega, z) = \int_{\widetilde{F}} G(\omega, k)\, e^{-jkz} \frac{dk}{2\pi}. \tag{9}$$

The Laplace contour (integration over ω) can be deformed to a line just below the real ω axis if there are no absolute instabilities. The deformed Fourier contour, $\widetilde{F}$, properly accounts for any poles of $G(\omega, k)$ (zeros of the dispersion equation) crossing the real k axis as the frequency is brought up from the Laplace contour ($\operatorname{Im} \omega \leqslant -\sigma_o$) to the real ω axis.

The function $F(\omega, z)$ can be written as a sum over the "normal modes" by evaluating the integral in Eq. 9 as a sum of residues:

$$F(\omega, z) = \sum_{k_{n+}} \frac{-j}{\left(\dfrac{\partial G^{-1}}{\partial k}\right)_{k=k_{n+}(\omega)}} \exp(-jk_{n+}(\omega)z), \quad z > 0$$

$$= \sum_{k_{n-}} \frac{j}{\left(\dfrac{\partial G^{-1}}{\partial k}\right)_{k=k_{n-}(\omega)}} \exp(-jk_{n-}(\omega)z), \quad z < 0. \tag{10}$$

The roots of the dispersion equation entering for $z > 0$ (k_{n+}) are those that appear to decay in space for a frequency on the Laplace contour $(Im \, \omega < -\sigma_o)$. If any of these roots have $Im \, k_{n+} > 0$ for a real frequency, then they appear as spatially growing (amplifying) waves. (Similar remarks apply to the case $z < 0$.)

If we drive the system sinusoidally in time, that is, if $f(t) = e^{j\omega_o t}$ for $t > 0$, then the asymptotic response of the system is

$$\lim_{t \to \infty} \psi(t, z) \to F(\omega_o, z) \, e^{j\omega_o t}. \tag{11}$$

That is, the function $F(\omega, z)$ represents the steady-state response of the system at the frequency ω. This steady-state response cannot contain any amplifying waves unless a solution of complex ω (with $\omega_i < 0$) for real k is obtained from the dispersion equation, in other words, unless the system supports "unstable waves." Our present task is to demonstrate that this condition is also _sufficient_, that is, that in a system supporting "unstable waves" (and free from absolute instabilities) there must be amplifying waves for some real frequency.

To show this, we shall use the results derived above for the asymptotic response to an impulse in time $(f(t) = \delta(t)$ and $f(\omega) = 1)$ in the limit as t and z approach infinity in a fixed ratio. In the present formalism, the response in the limit $t = z/V \to \infty$ is given by

$$\psi(t, z_o) = \sum_{k_{n+}} \int_{-\infty}^{\infty} \frac{-j}{\left(\dfrac{\partial G^{-1}}{\partial k} \right)_{k_{n+}}} \exp(-jk_{n+} z_o) \, \exp[j(\omega - k_{n+}(\omega)V)t] \frac{d\omega}{2\pi} \tag{12}$$

(from Eqs. 1, 8, and 10). We consider explicitly only the case $V > 0$ and amplification in the $+z$ direction; similar remarks also apply to the case $z < 0$ and $V < 0$.

The restriction that the system be free from absolute instabilities allowed us to carry out the ω integration along the real ω axis in Eq. 12. Since we know from our analysis that for $V = V_o$ this response increases as $\exp(\sigma_o t)$ as $t \to \infty$, we see from Eq. 12 that at least one of the normal modes (k_{n+}) must be an amplifying wave over some band of real frequency for the integral in Eq. 12 to diverge as $t \to \infty$. In fact, for $V = V_o$ the integral in Eq. 12 will increase _slower_ than $\exp(a_M V_o t)$, where a_M is the maximum $Im \, k_+$ for real ω (Fig. XI-26). We have therefore established the following lower bound on the maximum amplification rate (of a system free from absolute instabilities).

$$a_M > \frac{\sigma_o}{V_o} = \frac{\max(-\omega_i) \text{ for real } k}{(\partial \omega_r / \partial k) \text{ at } \max(-\omega_i)}. \tag{13}$$

The exact evaluation of the asymptotic limit of $\psi(t, z_o)$, from Eq. 12, could be done

in principle by a saddle-point technique. In this method, the dominant contribution to the integral comes from integrating through the points of stationary phase, with

$$1 - \frac{\partial k(\omega)}{\partial \omega} V = 0. \tag{14}$$

Note that choosing the "velocity" V equal to V_M (Fig. XI-26) will make the point $k = k_{rM} + j\alpha_M$, $\omega = \omega_M$, a point of stationary phase; hence, for this velocity the response
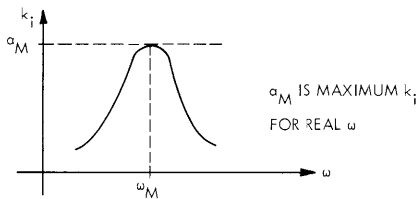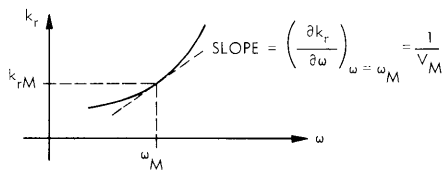

Fig. XI-26. Sketch of complex k for real ω.

will increase as $\exp(\alpha_M V_M t)$ as $t \to \infty$. Since we have shown that no velocity could cause the response to increase faster than $\exp(\sigma_o t)$, we can state the following upper bound on the amplification rate.

$$\alpha_M < \frac{\sigma_o}{V_M}. \tag{15}$$

In proving that this is an upper bound, however, we have made use of the fact that $\partial k_i / \partial \omega = 0$ at the maximum of $k_i(\omega)$ for real ω. Therefore we have actually assumed in this proof that the amplification rate is less than infinity, since the zero derivative of $k_i(\omega)$ at the maximum would not be true for a case in which k_i has a pole at ω_M. Such cases are sometimes obtained when very idealized models of the system are used.

R. J. Briggs

References

1. A. Bers and R. J. Briggs, Criteria for determining absolute instabilities and distinguishing between amplifying and evanescent waves, Quarterly Progress Report No. 71, Research Laboratory of Electronics, M. I. T., October 15, 1963, pp. 122-131.

G ELECTRON-CYCLOTRON RESONANCE DISCHARGE[*]

The low-pressure region of operation has been the subject of the experimental investigation since the last quarterly report.[1] Of particular interest were the characteristics of the x-rays and the cyclotron radiation produced by the discharge.

1. X-Ray Characteristics

The pattern of the x-rays produced at the cavity end walls was studied by using the x-ray pinhole camera technique. We found that the x-rays produced at the end walls came from a ring-shaped area. The diameter of the ring of x-rays can be changed by varying
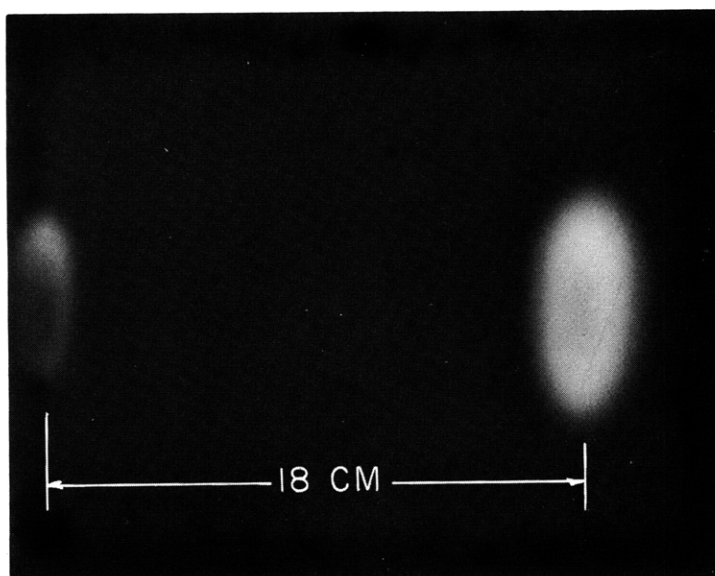

Fig. XI-27.

the strength of the steady magnetic field. The ring diameter increases with the steady magnetic field. Figures XI-27 and XI-28 are x-ray pinhole photographs of the discharge.

Figure XI-27 shows the x-rays coming from the two cavity end walls. The right cavity wall is a much more intense x-ray source than the left. This is explained by the fact that the cavity walls are not symmetrically located with respect to the center of the magnetic mirror. The field strength at the right wall is approximately 3 per cent less than that at the left wall.

Figure XI-28 shows an expanded picture of the x-rays produced at the right wall with 90 amps in the magnet coils. The diameter of this ring is 7.5 cm. These pictures were taken at a pressure of 10^{-5} torr with 50 kw peak microwave input power to the discharge.
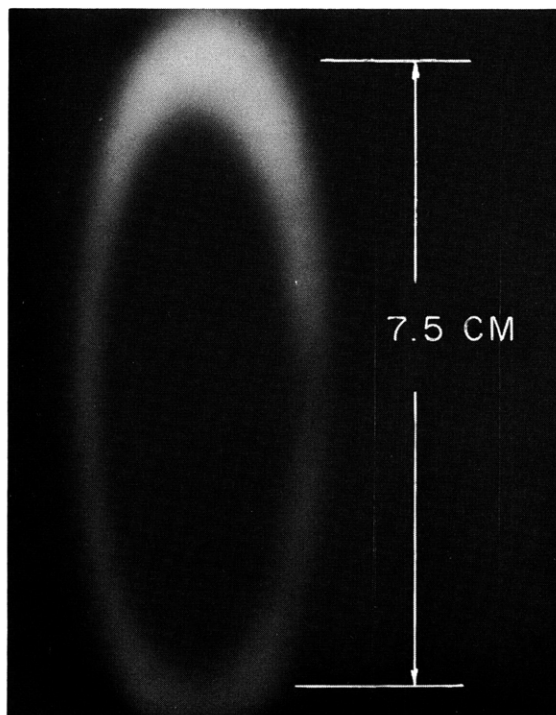

Fig. XI-28.

The presence of these rings indicates that the heating zone inside the cavity is well defined and can possibly be found by projecting the rings on the cavity walls along the magnetic field lines until they cross the 1000-gauss heating contour.

2. Cyclotron Radiation

Further observations of the cyclotron radiation produced by the plasma have shown an interesting time structure in the radiation. Between two microwave power pulses the cyclotron radiation either is not present or occurs as a series of 5-10 sharp bursts of less than 5-μsec duration. The experimentally determined probability of the cyclotron radiation being present between any two microwave power pulses is 0.5. When detected, the first burst of radiation occurs approximately 400 μsec after the microwave power pulse. The succeeding pulses are then of lower amplitude and occur at increasingly shorter time intervals until the next microwave power pulse. Spectrum analysis of these bursts has shown that the principal radiation occurs in the frequency band 2800 ± 300 mc.

T. J. Fessenden

References

1. T. J. Fessenden, Electron-cyclotron resonance discharge, Quarterly Progress Report No. 73, Research Laboratory of Electronics, M.I.T., April 15, 1964, pp. 72-80.

H. FEASIBILITY OF PULSED CONTROLLED FUSION POWER

A number of studies have been made of steady-state or quasi steady-state controlled fusion devices[1-4] as net power producers. These studies presuppose virtually complete plasma stability. That is, the plasma is assumed to be stable against both gross insta- bilities and the microinstabilities that lead to weak turbulence and enhanced diffusion across the confining magnetic field.

In this report we consider briefly some factors that will affect the feasibility of fusion power, if complete stability cannot be achieved. That is, we explore some of the pos- sible parameters of a pulsed fusion system.
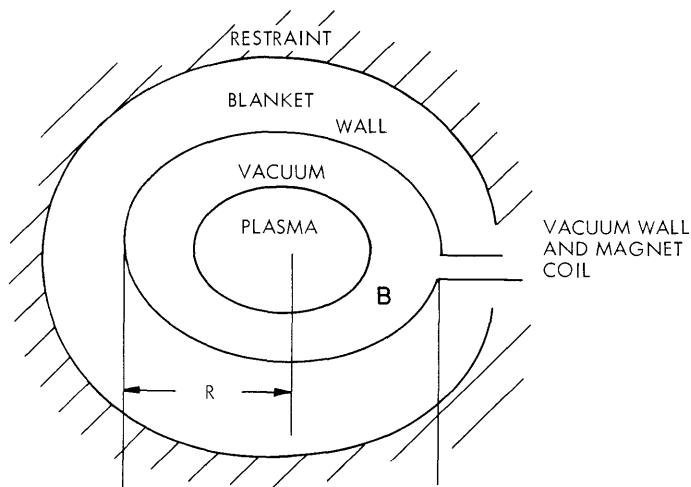

Fig. XI-29. Generalized pulsed system.

For our model, we take Fig. XI-29, which is a generalized pulsed system. As shown, it can be interpreted as a "theta pinch," but such an interpretation is not essential.

The main points are:

(i) The plasma is heated by some compression process to a desired temperature, and confined by a magnetic field for a time determined by plasma stability.

(ii) The coils are inside the energy-recovery blanket because a pulsed field cannot be applied through the blanket.

(iii) All of the nuclear energy, as well as the input plasma and magnetic field energy, is removed as heat. The neutron energy can only be removed as heat, and any attempt to remove directly the heat of the charged reaction products, the plasma or the magnetic field, as electric energy would lead to a shorter confinement time and less over-all output.

(iv) The plasma is deuterium and tritium. For a given value of the magnetic field

strength B and $\beta = 1$, the D-T reaction rate is orders of magnitude higher than any other rate (for example D-D), since the cross section is higher and the required ion temperature is lower, both factors allowing a higher density.[5] Also, the D-D power output is not significantly greater than the Bremsstrahlung power loss from the plasma at any temperature, thereby making it difficult to keep a D-D plasma hot long enough to produce a significant amount of nuclear energy.

(v) Use of a D-T reaction means that tritium will have to be regenerated in the blanket by reactions such as $Li^6 + n \rightarrow He^4 + T$, and (n, 2n) reactions are required to make up for neutrons absorbed in nontritium-producing reactions.

(vi) The neutron flux required for tritium regeneration limits the thickness of the coils.

As a result of these and other considerations, we can apply requirements to the system. There are five obvious ones.

(i) The wall strain cannot exceed a maximum allowable limit if the system is to be pulsed a large number of times without breaking. Here, we shall take a relative strain of 7×10^{-4} for M_o.

(ii) Turbulent diffusion: The distance that the plasma diffuses into the magnetic field during the pulse should be small compared with the confining chamber radius R to prevent sputtering damage to the wall and to keep the plasma hot. We assume a turbulent diffusion coefficient D of the form[6]

$$D = A\frac{kT_e}{eB},$$

which leads to a diffusion distance $\delta_B = \sqrt{4Dt}$. Here, k is the Boltzmann constant, T_e is the electron temperature, e is the charge on the electron, t is the time since the start of the pulse, and A is a variable coefficient corresponding to the mean-square density fluctuation in the plasma.

(iii) Wall heating: We allow a maximum temperature rise of 1000°C in the wall during the pulse. If the initial temperature is 400°C, this gives a final temperature of 1400°C, at which point molybdenum loses strength rapidly,[7] and its vapor pressure becomes high enough to cause appreciable vaporization.[8]

(iv) Energy: The ratio of the nuclear heat out to the total energy in must exceed some number r; r must be at least 3, since the efficiency of converting the heat output into input electric energy is only approximately 30 per cent.

(v) Wall thickness: We allow a maximum thickness of 3 cm of molybdenum for the wall, because of the tritium regeneration requirement.[3]

These requirements lead to the following limitations on B, R, and τ, the length of the pulse.

(i) Wall strain: We assume a completely rigid blanket wall outside the blanket and

assume quasi-static loading of the vacuum wall. At the beginning of the pulse, the vacuum wall is pushed outward, and hence the blanket fluid is compressed, until the pressure of the blanket fluid on one side of the blanket wall balances the driving magnetic pressure.

The wall stress is

$$\frac{B^2}{2\mu_o} = \frac{1}{\beta_B} \frac{\Delta V_B}{V_B},$$

where β_B is the volume compressibility of the blanket. For a rough estimate, we take $\beta_B = 2.3 \times 10^{-11}$ m^2/newton. We assume a thickness of 1 meter for the blanket. Then

$$\frac{B^2}{2\mu_o} < 0.0007 \frac{R}{\beta_B}. \tag{1}$$

(ii) Turbulent diffusion: $\rho_B < R/3$, or

$$\frac{R^2}{\tau} > 4 \times 9 \frac{kT_e}{eB}. \tag{2}$$

(iii) Wall heating:

$$\rho C_V \Delta T_{max} > E_N + E_{Br} + E_B, \tag{3}$$

where

$\rho = 10.2$ gm/cm^3 = density of wall material (Mo),

$C_V = 3.14 \times 10^6$ erg/gm °C at 20°C = heat capacity of Mo.

We shall assume $\Delta T_{max} = 1000°C$, and take

$$E_N = \frac{10B^4 <\sigma v_{DT}> Rf\tau e_n}{128\mu_o^2 (kT)^2}$$

as the energy per unit volume left in the wall by the neutrons, under the assumption that the neutrons lose 10 per cent of their energy per centimeter of Mo through which they pass.[4] We shall also take

$$T = T_{electron} = T_{ion} = 20 \text{ kev.}$$

Here, $\langle \sigma v_{DT} \rangle = 4.4 \times 10^{-22}$ m^3/sec = the average value of the D-T cross section times the relative velocity of the ions for an ion temperature of 20 kev; f = the fraction of the volume of the confining chamber occupied by the plasma; $e_n = 14.1$ Mev = the energy of the neutrons; and

$$E_{Br} = \frac{4.8 \times 10^{-37} \, B^4 T_e^{1/2} R f \tau^{1/2}}{32 \mu_o^2 (kT)^2} \sqrt{\frac{\rho e_V}{2K}}$$

is the energy per unit volume absorbed on the surface of the wall from Bremsstrahlung, with the power radiated by the plasma given by

$$P_{Br} = 4.8 \times 10^{-37} \, n^2 T_e^{1/2} \text{ watts/m}^3$$

$T_e = 20$, the electron temperature in kev

$K = 0.28$ cal/sec cm °C at 20°C, the thermal conductivity of Mo.

$$E_B = \frac{B^2}{2\mu_o}$$

is the heat added to the wall, because of the penetration of the magnetic field. The heating caused by cyclotron radiation would probably also be significant, but is neglected in this first approximate calculation.

(iv) Energy: $E_{Th} > 3E_{in}$,

$$E_{Th} = \frac{1}{4} n_i < \sigma v_{DT} > \pi R^2 f \tau e_{Th} \tag{4}$$

is the nuclear energy output per unit length; n_i is the ion density; $e_{Th} = 22.4$ Mev is the energy released per D-T reaction, 17.6 Mev, plus the energy of the $Li^6 + n$ reaction, 4.8 Mev.

$$E_{in} = \frac{B^2}{2\mu_o} \pi R^2 \left(1 + \frac{1}{2} f\right) \approx \frac{\pi R^2 B^2}{2\mu_o} \qquad \text{for } f \ll 1$$

is the energy per unit length of the magnetic field and the plasma. For an isotropic velocity distribution, the energy density in a $\beta = 1$ plasma is 3/2 times the energy density in the confining field.

Inserting numerical values for the physical constants and setting $A = 0.05$ A' and $f = 0.10$ f' (in order to use A' and f' both ≈ 1), we find the limitations in terms of R in meters, τ in seconds, and B in webers/m^2:

Turbulent diffusion: $\quad \dfrac{BR^2}{\tau} \gg 3.6 \times 10^4 \, a' \tag{5}$

Wall heating: $\quad 1 > 3.4 \times 10^{-4} \, f' B^4 R \tau \left(1 + \dfrac{1}{10\sqrt{\tau}}\right) + 1.25 \times 10^{-4} \, B^2 \tag{6}$

Energy: $\quad B^2 \tau > \dfrac{3.5}{f'} \tag{7}$

$$r = E_{Th}/3E_{in} = .28 f' B^2 \tau \tag{8}$$

Wall strength: $\quad \dfrac{B^2}{R} < 78 \tag{9}$

The dynamic loading effects of the inertia of the wall and the blanket material were also considered, but it was found that for reasonable sizes (R≪100 meters) and for values of

B and τ large enough to satisfy the energy requirements (Eq. 8) the strain would greatly exceed 0.0007 without the effects of the compression of the blanket. Also, the loop strength is insufficient for values of R, τ, and B that satisfy the energy and turbulent-diffusion requirements.

Combination of the diffusion, heating, and energy requirements, Eqs. 5, 6, and 7, under the assumption that $\tau > 0.01$ sec (so that $1 + (1/10\sqrt{\tau}) \to 1$ in Eq. 6) gives

$$R > 27A'^2/f'^2 \tag{10}$$

$$\tau > 0.11A'^2/f'^3 \tag{11}$$

$$B < 5.6f'/A'. \tag{12}$$

For A' and f' near 1 (f'/A'<2.8), any values of R and B that satisfy Eqs. 10 and 12 also satisfy the strength requirement, Eq. 9.

For $\tau > 1$ and B $\ll$ 100, so that Eq. 6 takes the form

$$1 > 3.4 \times 10^{-4} f'B^4R\tau.$$

The heating, diffusion, and strength requirements limit $r = E_{Th}/3E_{in}$ to

$$r < 5.4 \times 10^{-3} \frac{f'}{A'} R^{7/2}. \tag{13}$$

For values f' = 2, A' = 0.2, and R = 5 meters, Eq. 13 gives

$$r < 14E_{Th} < 42E_{in}.$$

Given diffusion rates of the same order of magnitude as those that have already been achieved in small experiments, a pulsed thermonuclear device of reasonable size which will produce more power than it consumes may be possible. Decrease in the diffusion rate leads to rapid decrease in the minimum size of such a device and rapid increase in the ratio of power out to power in for a given size.

F. E. Dunn, D. J. Rose

References

1. R. F. Post, Revs. Modern Phys. 28, 338 (1956).

2. D. J. Rose and M. Clark, Plasmas and Controlled Fusion (The M.I.T. Press, Cambridge, Mass. and John Wiley and Sons, Inc., New York, 1961).

3. A. J. Impink, Neutron Economy in Fusion Reactor Blanket Assemblies, Ph.D. Thesis, Department of Nuclear Engineering, M.I.T., 1963.

4. W. G. Homeyer, Thermal and Chemical Aspects of the Thermonuclear Blanket Problem, Sc.D. Thesis, Department of Nuclear Engineering, M.I.T., 1963.

5. D. J. Rose and M. Clark, op. cit., p. 19.

6. S. Yoshikawa and D. J. Rose, Phys. Fluids 5, 344 (1962).

7. B. L. Mordike, Inst. Metals J. 88, 272 (1960).

8. D. J. Rose and M. Clark, op. cit., p. 302.

9. Ibid., p. 315.

I. BREMSSTRAHLUNG SPECTRUM OF HOT ELECTRONS[*]

Preliminary studies of the Bremsstrahlung spectrum from hot electrons in the electron-cyclotron heating experiment have been carried out. The expected exponential decrease with energy of the photon flux has been observed at pressures above 10^{-5} torr. At low pressures (around 3×10^{-6} torr), however, the observed spectrum may have as many as three peaks, the number depending on the strength of the magnetic field.

T. S. Brown

J. DETERMINING THE ELECTRON DISTRIBUTION FUNCTION FROM SCATTERED LIGHT[*]

Plasma diagnostic techniques utilizing scattered optical radiation, which are now being developed,[1] permit, in principle, detailed measurements of the electron velocity distribution function. The expression giving the electron velocity distribution function in terms of the spectral intensity of the scattered light has been derived and will be reported here.

The spectral intensity is expressed in terms of the distribution function under the following assumptions. Quantum-mechanical effects and scattering from ions are neglected. Collisions are also neglected, only electron accelerations caused by the incident radiation being considered. The distribution function in the region that is observed is assumed not to change during the measurement. The electrons are assumed to be distributed randomly and to scatter incoherently so that the scattered powers are additive. The intensity of the incident radiation, I_o, is assumed to satisfy the condition

$$I_o \ll \frac{\pi}{2} \frac{E}{\lambda_o^2 (r_e/c)} (1 - \underline{n}_o \underline{\beta}),$$

where $E \ (= \gamma mc^2)$ is the total energy of the electron, and $\beta \ (= \underline{v}/c)$ is its unperturbed velocity, $\underline{n}_o$ is a unit vector in the direction of propagation of the incident radiation of wavelength λ_o and frequency ω_o, and r_e is the classical radius of the electron.

Under these conditions it can be shown that

$$s(\underline{n}, \omega) = \frac{3}{8\pi} \sigma_T n_e I_o \frac{\omega^2}{\omega_o^3} \int d\underline{\beta} \ f(\underline{\beta}) \ \delta(g(\underline{n}, \omega, \underline{\beta})) \ K(\underline{n}, \underline{\beta}), \tag{1}$$

where $s(\underline{n}, \omega)$ is the power per unit frequency interval scattered into a unit solid angle in the direction of the unit vector $\underline{n}$, σ_T is the Thomson cross section of an electron,
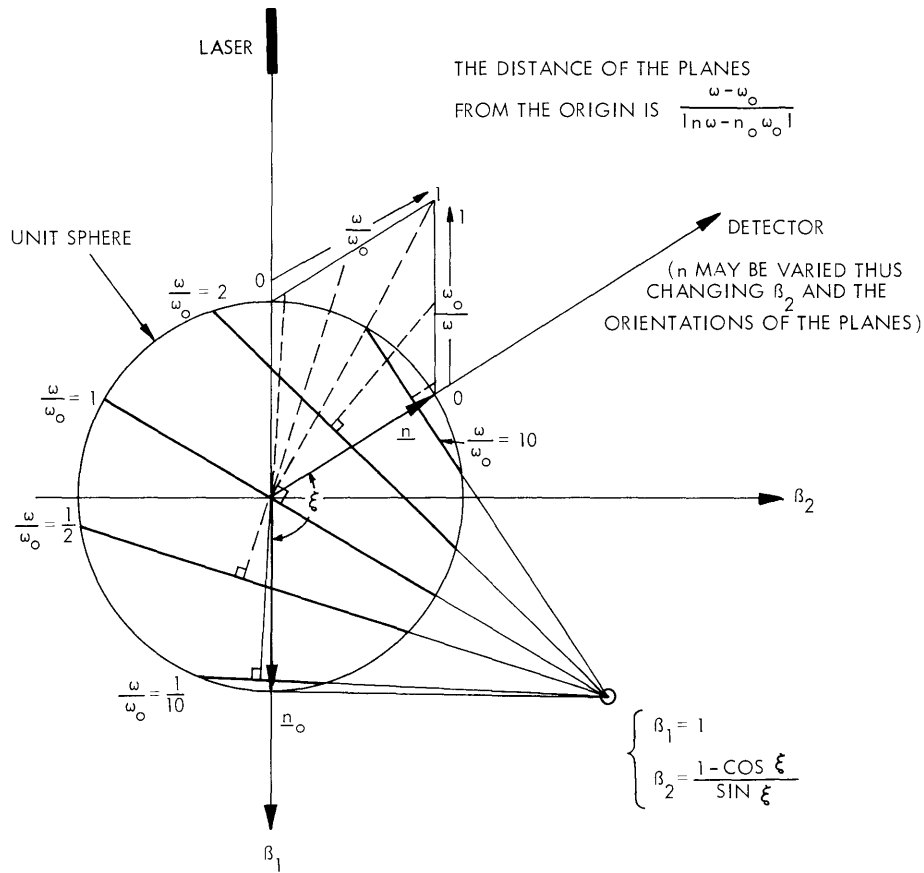
Fig. XI-30. Planes in $\underline{\beta}$ space that contribute to the spectral intensity at definite frequencies.

n_e is the number density of electrons, $f(\underline{\beta})$ is the electron velocity distribution function normalized so that

$$\int d\underline{\beta}\ f(\underline{\beta}) = 1,\tag{2}$$

and the argument of the Dirac delta function $(g(\underline{n},\omega,\underline{\beta}))$ and $K(\underline{n},\underline{\beta})$ are defined by

$$g(\underline{n},\omega,\underline{\beta}) = \frac{1}{\omega_o}[\underline{\beta}\cdot(\underline{n}\omega - \underline{n}_o\omega_o)-(\omega - \omega_o)]$$

and

$$K(\underline{n},\underline{\beta}) = (1-\beta^2)\left[d_1 + d_2\frac{\beta^2(\hat{E}\cdot\hat{v})^2}{(1-\underline{n}_o\cdot\underline{\beta})^2} - d_3\frac{2\frac{\gamma-1}{\gamma}(\hat{E}\cdot\hat{v})}{(1-\underline{n}_o\cdot\underline{\beta})}\right].$$

Here,

$$d_1 = 1 - (\hat{E} \cdot \underline{n})^2$$

$$d_2 = 1 - (\underline{n}_o \cdot \underline{n})^2$$

$$d_3 = (\underline{n} \cdot \hat{E})(\underline{n} \cdot \hat{v}).$$

$\hat{E}$ is a unit vector in the direction of the electric field, and $\hat{v}$ is a unit vector in the direction of $\underline{\beta}$.

The delta function picks out the planes in $\underline{\beta}$ space which contribute to the spectral intensity at $\underline{n}$ and ω, and $K(\underline{n}, \beta)$ weights the various regions of each plane. The construction of these planes from $g(\underline{n}, \omega, \beta)$ is illustrated in Fig. XI-30. Similarly, $g(\underline{n}, \omega, \beta)$ defines the prolate spheroids in $\underline{k}$ $(= \underline{n}\omega)$ space to which and only to which an electron with velocity β contributes scattered radiation. These spheroids are illustrated in Fig. XI-31.

LENGTH OF MAJOR AXIS $= 2k_o \, (1 - \beta \cdot \underline{n}_o)$
LENGTH OF MINOR AXIS $= 2k_o \, (1 - \beta \cdot \underline{n}_o)$
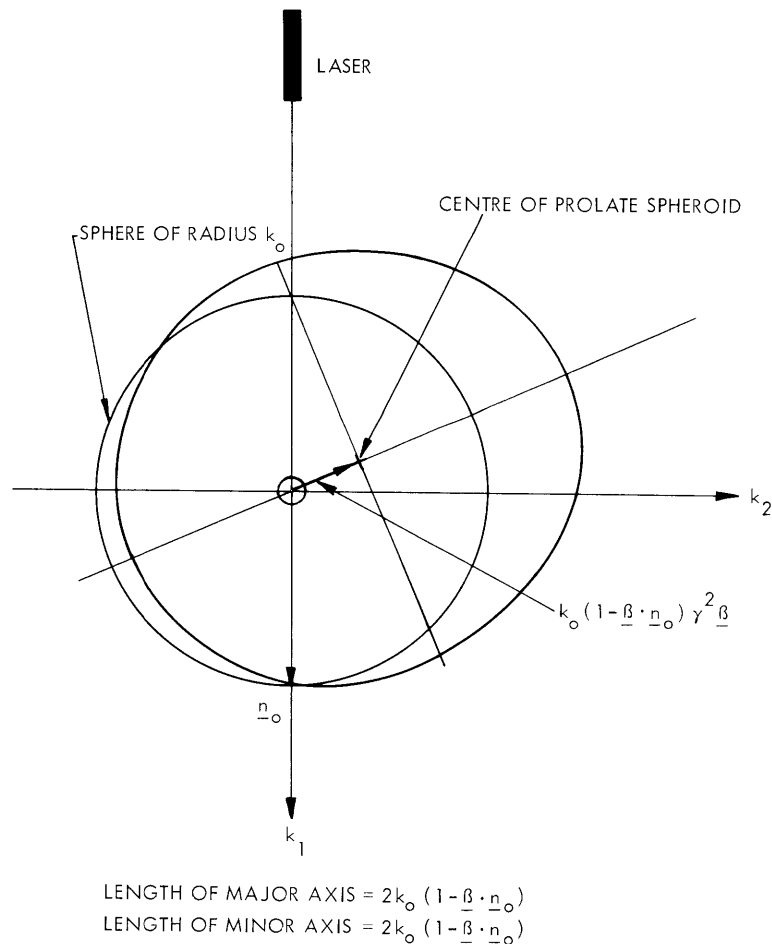
Fig. XI-31. Prolate spheroid in $\underline{k}$ space to which an electron scatters incident radiation.

The solution of Eq. 1 in the nonrelativistic limit can be shown to be

$$f(\underline{\beta}) = -\frac{2}{3\pi} \Delta_{\beta} \int_{\frac{1}{2}\Omega_a} ds_a \left[\frac{s(\underline{n}, \omega) |\underline{n}\omega - \underline{n}_0 \omega_0|}{\sigma_T n_e I_0 \frac{\omega^2}{\omega_0^2} (1 - (\hat{E} \cdot \underline{n})^2)} \right],$$

where $\underline{n}$ and ω in the integrand are to be replaced by

$$\underline{n} = \underline{n}_0 - 2(\underline{a} \cdot \underline{n}_0) \underline{a}$$

$$\omega = \omega_0 (1 - 2(\underline{a} \cdot n_0)(\underline{a} \cdot \underline{\beta})),$$

and Δ_{β} is the Laplacian with respect to $\underline{\beta}$, $\underline{a}$ is a unit vector, and ds_a is the differential of area (in $\underline{a}$ space) of the hemisphere $\frac{1}{2} \Omega_a$ centered on $\underline{n}_0$.

T. S. Brown

References

1. E. Thompson and G. Fiocco, Scattering of light from (plasma) electrons III, Quarterly Progress Report No. 69, Research Laboratory of Electronics, M.I.T., April 15, 1963, pp. 74-80.